



This is a repository copy of *Paper of RILEM TC 282-CCL: mineralogical characterization methods for clay resources intended for use as supplementary cementitious material*.

White Rose Research Online URL for this paper:

<https://eprints.whiterose.ac.uk/188148/>

Version: Accepted Version

Article:

Snellings, R., Almenares Reyes, R., Hanein, T. orcid.org/0000-0002-3009-703X et al. (7 more authors) (2022) Paper of RILEM TC 282-CCL: mineralogical characterization methods for clay resources intended for use as supplementary cementitious material. *Materials and Structures*, 55 (5). 149. ISSN 1359-5997

<https://doi.org/10.1617/s11527-022-01973-1>

This is a post-peer-review, pre-copyedit version of an article published in *Materials and Structures*. The final authenticated version is available online at:
<http://dx.doi.org/10.1617/s11527-022-01973-1>

Reuse

Items deposited in White Rose Research Online are protected by copyright, with all rights reserved unless indicated otherwise. They may be downloaded and/or printed for private study, or other acts as permitted by national copyright laws. The publisher or other rights holders may allow further reproduction and re-use of the full text version. This is indicated by the licence information on the White Rose Research Online record for the item.

Takedown

If you consider content in White Rose Research Online to be in breach of UK law, please notify us by emailing eprints@whiterose.ac.uk including the URL of the record and the reason for the withdrawal request.



eprints@whiterose.ac.uk
<https://eprints.whiterose.ac.uk/>

Paper of RILEM TC 282-CCL: Mineralogical characterization methods for clay resources intended for use as supplementary cementitious material

Ruben Snellings^{1*}, Roger Almenares Reyes², Theodore Hanein³, Edgardo F. Irassar⁴, Fragkoulis Kanavaris⁵, Matthias Maier⁶, Alastair T. Marsh⁷, Luca Valentini⁸, Franco Zunino⁹, Adrian Alujas Diaz¹⁰

1 Sustainable Materials, VITO, Mol, Belgium

2 Instituto Superior Minero Metalúrgico de Moa, Moa, Cuba

3 Department of Materials Science and Engineering, University of Sheffield, UK

4 Departamento de Ingeniería Civil, National University of the Center of the Buenos Aires Province, Argentina

5 ARUP, London, UK

6 University of the Bundeswehr Munich, Neubiberg, Germany

7 School of Civil Engineering, University of Leeds, Leeds, UK

8 Department of Geosciences, University of Padua, Padua, Italy

9 Laboratory of Construction Materials, École Polytechnique Fédérale de Lausanne, Lausanne, Switzerland

10 Centro de Estudios de Química Aplicada, Universidad Central de Las Villas, Santa Clara, Cuba

*corresponding author: Ruben Snellings, ruben.snellings@vito.be

Abstract

To respond to the rapid introduction and development of calcined clays as supplementary cementitious material (SCM), the toolbox of characterization methods for cementitious materials requires extension to raw clay characterization. Borrowing concepts and methods developed in the field of clay mineralogy, this paper outlines the merits and limits of widely accessible characterization techniques for raw clays intended for use as SCM, when calcined. The paper focuses mainly on the identification and quantification of the raw clay mineral components, as these characteristics have important implications for further material processing and performance. General notes are provided on clay sampling and pre-treatment as well as bulk chemical analysis. The main techniques considered are X-ray diffraction, thermal analysis and infrared spectroscopy. Their application on raw clays is introduced, highlighting clay-specific aspects of sample preparation, data acquisition, and processing. Guidelines and interpretation tables are provided to aid in the analysis of the acquired data, while limitations and potential interferences are identified. Options for remote prospection by infrared spectroscopy are included as well. To illustrate the type of information to be gained and the complementarity of the techniques, two representative raw clays are fully characterised. This paper aims to highlight that mineralogical characterization is a feasible and often necessary step in the study and assessment of raw clays that can deliver a wealth of informative data if carried out appropriately.

Key words: Clay, Characterisation, Mineralogy, Cement, Supplementary Cementitious Materials

This paper has been prepared by working group 1 within RILEM TC 282-CCL. The paper has been reviewed and approved by all members of the TC.

TC Membership

46 Chair: Prof. Fernando Martirena-Hernandez

47 Deputy Chair: Prof. Manu Santhanam

48 Members: Sumaiya Afroz, Laith Al-Jaberi, Adrian Alujas-Diaz, Francois Avet, Tushar Bansal, Hoda
49 Beltagui, Mohsen Ben Haha, Susan Bernal Lopez, Shashank Bishnoi, Pascal Boustingorry, Mariana
50 Canut, Arnaud Castel, Vinh Dao, Frank Dehn, Yuvaraj Dhandapani, Pascal Dion, Jan Elsen, Gilles
51 Escadeillas, J Ivan Escalante-Garcia, Hassan Ez-Zaki, Sergio Ferreira Garzón, Daniel Geddes, Guoqing
52 Geng, Ravindra Gettu, Theodore Hanein, Edgardo Irassar, Roman Jaskulski, Shiju Joseph, Maria C.
53 Garcia Juenger, Sri Kalyana Rama Jyosyula, Fragkoulis Kanavaris, Taehwan Kim, Wolfgang Kunther,
54 David Law, Alisa Machner, Matthias Maier, Alastair Marsh, Fabrizio Moro, Joseph Mwiti Marangu,
55 Angela Nunes, Katelyn O Quinn, Anuj Parashar, Gabriel Pham, Victor Poussardin, John Provis, Elsa
56 Qoku, Kyle Riding, Roger Almenares Reyes, Karyne Ferreira dos Santos, Karen Scrivener, Jorgen
57 Skibsted, Ruben Snellings, Tongbo Sui, Arezki Tagnit-Hamou, Karl-Christian Thienel, Luca Valentini,
58 Oscar Oswaldo Vazquez, Luis Velasquez, Manuel Vieira, Silvia Vieira, Talakokula Visalakshi, Claire
59 White, William Wilson, Kequan Yu, Zengfeng Zhao, Wenzhong Zhu, and Franco Zunino.

60
61

62 Contents

63	1. Introduction	2
64	2. Sampling and pre-treatment of raw clays	3
65	3. Characterisation techniques for qualitative and quantitative analysis	4
66	3.1. Chemical analysis techniques	4
67	3.2. X-ray powder diffraction	5
68	3.3. Thermal analysis.....	10
69	3.4. Vibrational spectroscopy	16
70	4. Case studies	22
71	5. Summary and perspectives.....	25

72

73 1. Introduction

74 Relevant and reliable data are a cornerstone of scientific progress and industrial or governmental
75 decision-making. Acquisition, processing, and interpretation of raw data are therefore key aspects of
76 scientific practice and most disciplines have developed tailored sets of test methods and techniques
77 adapted to the field of study. This set of tests is subject to continuous adaptation in response to
78 technical developments and extensions or shifts of scope of the field.

79 Current developments towards low carbon cements have spurred the introduction of calcined clays
80 for use as SCMs [1-3]. To suit exploration and extraction purposes, there is a need to extend the
81 cement producer's toolbox with reliable and informative characterization techniques, robust towards
82 the natural diversity and complexity of common and impure clays [4-6].

83

84 Clays have always been tedious materials to characterize in terms of composition and microstructure.
85 The, by definition, fine-grained nature of clays and their mineralogical complexity made it difficult to
86 study them using classical geological tools, such as optical microscopy. It was mainly the introduction
87 of X-ray powder diffraction that led to the development of clay mineralogy [7, 8]. Complemented by

88 chemical analysis, thermogravimetric analysis and spectroscopic techniques, and combined with
89 powerful computational tools, clay mineralogists are now able to quantitatively determine the
90 mineralogical make-up of clays to an unprecedented level of detail. Outstanding exploits of analytical
91 prowess are featured in the so-called Reynold's Cup, a bi-annual global contest in quantitative
92 mineralogical analysis of clays, where laureates succeed in accurately analysing challenging synthetic
93 clay samples comprising up to 30 different mineral phases [9, 10].
94

95 Recent advances in clay mineralogical analysis were mainly driven by extractive industries. In
96 particular, oil and gas exploration has exploited the complex and characteristic mineralogy of clays as
97 a fingerprint for decoding reservoir rock sequences or hydrocarbon source rock maturity [11]. Other
98 industries have focused on more accessible characteristics such as bulk chemical composition or
99 colour to define acceptance criteria. Recent work has shown that the reactivity and performance of
100 calcined clays as SCM depend strongly on the mineralogical composition of the raw clay, and that low
101 grade kaolinitic (30-40 wt.% kaolinite) and other common, impure clays can also show acceptable
102 cementitious properties after calcination [12-16]. Whilst several key texts exist for specific techniques
103 and clay characterisation in a broad sense (these will be referenced throughout), these are largely
104 application-agnostic – a treatment for the most relevant techniques specific to clays as SCMs is
105 currently lacking. As such, this paper introduces key characterisation techniques for detailed clay
106 mineralogy analysis for the specific application of producing SCMs. X-ray diffraction, thermal analysis,
107 and infrared spectroscopy are selected as common techniques available in most resource or material
108 characterisation laboratories. These are discussed in terms of obtainable information, practical
109 implementation, and analysis and interpretation related to clays. Although, complementary
110 information with relevance to sampling and chemical analysis of clays are elaborated first.
111

112 2. Sampling and pre-treatment of raw clays

113 While the accuracy of modern analytical equipment is usually considered as the main source of
114 variation in materials characterization, this may not be true in many cases. If not properly executed,
115 sampling and sample preparation is a major source of variation and bias. For minerals that occur in
116 such diverse and heterogeneous environments such as clay minerals, a representative sampling and
117 an adequate understanding of the characteristics of the clay deposit are of paramount importance.
118 Any conclusions that may be derived from state-of-the-art characterization techniques are not
119 particularly meaningful unless one is certain that the sample is truly representative of the clay deposit
120 that is intended to be characterized. The final goal of any sampling should be to provide the analyst
121 with a homogeneous sample, representative of the lithological feature of interest at the predefined
122 spatial resolution.

123 A geological evaluation of a clay deposit aims to provide more detailed information about the area of
124 interest and raise confidence for industrial exploitation, moving from hypothetical resources to
125 proven reserves. In a geological survey a grid of sampling points should be established, adapted to
126 geomorphology and covering all relevant lithologies. A record should be made for every collected
127 sample, including lithological and textural descriptions. A spatial mapping of the occurring lithologies
128 is essential, as this provides indispensable information for resource volume estimations. The relevance
129 of this information should not be underestimated, as this supports the interpretation of sample
130 characterization results. Subsequent blending and homogenization of several samples together may
131 reduce the resolution of the field observations [17].

132 As a rule of thumb, the higher the heterogeneity of a clay deposit, the more sampling points are
133 required to obtain a representative averaged sample. All relevant lithologies present in a clay deposit
134 should be representatively sampled in more than one location. For common manual procedures, such
135 as shovelling or use of a hand auger, the surface should be cleaned before sampling to remove soil or

136 surface alterations and avoid cross-contamination between different lithologies. Composite samples,
137 representative of large areas, are generated by alternative sub-sampling of primary samples, taking
138 several small portions of approximately the same size from each individual sample. Afterwards, pre-
139 homogenization of composite samples is usually done by manual mixing procedures. Samples should
140 be stored in well-marked sturdy containers or bags to avoid accidental mixing or spillage of materials,
141 and mitigate moisture loss [17, 18].

142 Once clay samples arrive at the characterization facilities, they should be oven-dried at 105 °C to
143 remove moisture and make the material easier to handle and comminute. At the same time, the
144 moisture content of the clay can be measured. If the sample contains big chunks of clay it is
145 recommended to manually reduce them to cm-size before drying, otherwise moisture may be trapped
146 inside. A second step involves sample reduction up to approximately 1 mm. This step, usually done by
147 jaw crushers, disk mills or similar tools, is essential to guarantee further success in homogenization
148 and sample dividing steps. Coarse particles often have a somewhat different composition than finer
149 fractions, and may not get evenly distributed during sample splitting. The use of high energy grinding
150 or milling tools, such as planetary ball mills, is not recommended at this stage, as it may cause
151 undesirable structural changes to the clay minerals in the sample. In addition, care should be taken to
152 prevent dust losses during size reduction, otherwise the finest fraction could be underrepresented in
153 the final sample. Final steps in sample preparation involve homogenization and further division and
154 reduction of sample size. This could be done by manual (cone and quartering, sample splitters) or
155 automated procedures (rotating and rotary tube sample dividers). If available, the use of automated
156 procedures is recommended to reduce human bias [19].

157 Further steps regarding sample preparation for instrumental analysis, which usually involves grinding
158 to analytical fineness, separation of fine fractions, or sample digestion, are specific for each analytical
159 technique and will be discussed separately in the following sections.

160 3. Characterisation techniques for qualitative and quantitative analysis

161 3.1. Chemical analysis techniques

162 Determining elemental composition is a key part of characterisation that can inform and help
163 interpretation of other analytical techniques, as well as having specific value in its own right. Although
164 clays and associated minerals are structurally complex materials, chemical analysis of its major
165 components could be narrowed down to just a few elements: Si, Al, Fe, Mg, Ca, Na, K, Ti, Mn, S, P, and
166 Loss on Ignition (LOI) evolved above 105 °C. This range of chemical elements could be assessed by
167 most of the existing techniques, including standard methodologies involving wet chemistry methods.
168 However, due to its increased availability, accuracy and faster sample processing, it is not infrequent
169 that instrumental techniques such as X-ray Fluorescence (XRF), Atomic Absorption Spectroscopy (AAS)
170 or Inductively Coupled Plasma – Optical Emission Spectrometry (ICP-OES) are used for routine
171 chemical analysis in both industrial and research laboratories. Acknowledging that a plethora of other
172 techniques are available, a brief overview of XRF and ICP-OES is given here, as these techniques are
173 considered most relevant in the context of clay resource evaluation.

174 X-ray fluorescence (XRF) spectroscopy measures the characteristic energy (or wavelength) of X-ray
175 photons (fluorescence). This fluorescence is emitted when a higher energy electron makes a transition
176 to fill an inner shell vacancy, generated by the excitation of an inner shell electron by incident X-
177 radiation [20]. The fluorescence is measured and recalculated into element (or oxide) concentrations.
178 Laboratory-based XRF is a routine technique for mineral resource characterisation, usually conducted
179 alongside XRD. Sample preparation is key to obtaining reliable XRF results. The main options for
180 sample preparation are loose powders, pressed pellets and fused beads. Loose powders and pressed

181 pellets are more easy to prepare, however are less accurate and sensitive due to matrix effects (i.e.
182 the influence of neighbouring atoms in crystal structures on the measured energy spectrum [21]).
183 Matrix effects are reduced when fused beads are made by thermal melting the sample using a fluxing
184 material such as lithium metaborate. It is important to note that lighter and volatile elements (Na etc.)
185 evaporate during the preparation and cannot be measured this way [22]. In order to adjust for matrix
186 effects, it is recommend to generate a calibration curve using matrix-matched standards prepared in
187 the same way as the samples for measurement.

188 Recent developments of most interest have been in handheld or portable XRF (pXRF). More details on
189 pXRF instrumentation can be found elsewhere [20, 23, 24]. pXRF is truly portable, with handheld
190 devices that can produce a reading within a few minutes. It has extensively been applied to detection
191 of heavy metals in contaminated soils [25], but is also used in geochemical prospecting [26] and
192 measuring the $\text{SiO}_2\text{:Al}_2\text{O}_3$ ratio in soils [27, 28]. Drawbacks from in-field pXRF are reduced accuracy,
193 largely due to particle size and moisture content [25], with less effective detection for lighter elements
194 [20]. Nonetheless, pXRF has the potential to increase the flexibility and reduce costs of clay
195 prospecting by giving fast, in-situ measurements of key composition ratios.

196 Inductively coupled plasma optical emission spectroscopy (ICP-OES, also named ICP-AES, standing for
197 *atomic* emission spectroscopy) provides the bulk chemical composition of a solution, converted in
198 aerosol by means of a nebuliser and interacting with an argon plasma (5000-7000 K) that breaks the
199 aerosol sample into atoms and ions in an excited state [29]. As the system returns to a lower energy
200 state, radiation with a characteristic wavelength is emitted. The wavelength and intensity of the
201 emitted radiation depend on the chemical species present in the sample, and their concentration.
202 Quantification of the atomic species is obtained with the aid of calibrating solutions of known
203 concentrations [30].

204 When compared to XRF, ICP-OES provides better accuracy and sensitivity, particularly for elements
205 with low atomic numbers having low fluorescence yield. However, sample preparation is demanding,
206 as it requires the digestion (dissolution) of the solid sample in a solution [31]. Incomplete sample
207 dissolution is a common issue generating bias in the measurement, particularly in the case of certain
208 stable silicates (e.g. zircon) and oxides (e.g. rutile). For clays, common digestion techniques comprise
209 microwave assisted acid dissolution in which a combination of acids is used (e.g. concentrated HBF_4 ,
210 HNO_3 and HCl), or high temperature fusion with lithium metaborate followed by dissolution of the
211 resulting beads into nitric acid. As in case of preparation of fused beads for XRF, volatile anions (SO_3 ,
212 Cl , F ,...) and alkali cations (Na , K ,...) can be evaporated to a significant extent during high temperature
213 treatment. For these elements, acid digestion at low temperature followed by anion chromatography
214 or atomic absorption spectroscopy measurements provide more accurate determinations.

215 Low detection limits make this technique suitable for the analysis of contaminants in soil samples,
216 although last-generation XRF instruments proved reliable in providing comparable accuracies in the
217 chemical analysis of soils [32]. For heavy metal trace element analysis at the ppb level, ICP-mass
218 spectrometry (MS) is the reference. ICP-OES can be considered as the preferred method for studying
219 dissolution pathways of clay minerals used as SCM [33], rather than for prospecting purposes.

220 **3.2. X-ray powder diffraction**

221 X-ray powder diffraction is based on the interaction of X-rays that are scattered (also called reflected)
222 by crystal lattice planes¹. Unlike XRF, XRD relies the interference of elastically scattered X-rays, this

¹ These sets of parallel planes are usually referred to by their (hkl) or Miller indices. $1/h$, $1/k$ and $1/l$ define the intercepts of the planes with the a , b and c dimensions of the unit cell, respectively (e.g. (00l) reflections are parallel to the a - b basal plane).

223 means the detected X-rays have the same energy and wavelength as the source X-rays. Due to their
224 very small crystal size and complex crystal structures clay minerals are one of the most difficult types
225 of minerals to study. As a technique, X-ray diffraction (XRD) is regarded as one of the most informative
226 and important experimental techniques with relevance to the mineralogical analysis of clays to date,
227 providing insights hardly obtainable by other techniques [8]. XRD may even considered as
228 indispensable when it comes to accurate qualitative and quantitative clay analysis, and is a core
229 instrument in any clay mineralogy laboratory [34]. Invariably XRD has been the primary analysis
230 technique employed by the best performing participants in the Reynolds Cup, a bi-annual contest in
231 quantitative mineral analysis, with other techniques providing complementary, yet valuable
232 information [9].

233 Nevertheless, extracting accurate and detailed information from XRD measurements on clays is not
234 straightforward. It requires rigorous preparation techniques and careful analyses to distinguish and
235 identify clay minerals. More than for any other technique, specific sample preparation routines and
236 quantification approaches have been developed for XRD analysis of clays. In this respect, the advent
237 of ever more powerful computerized analysis in the last decades has revolutionized the field by
238 enabling structural simulations and accurate quantification of clay-bearing samples. This section
239 presents a succinct and selective introduction to the topic, providing the reader with an overview of
240 the methodology, where relevant illustrated by examples from case studies. For more advanced and
241 complete treatises on the topic the interested reader is referred to Brindley and Brown [7], Moore
242 and Reynolds [8] and Srodon [11].

243 **3.2.1. Sample preparation and data collection**

244 Sample preparation is of paramount importance with regards to correct identification of clay minerals
245 and quantitative phase analysis of clays. The neglect of oriented samples treated at different
246 conditions has been identified as one of the major error sources in quantitative phase analysis by
247 analyses of participant performance in the Reynolds Cup [9]. The different pre-treatments and
248 procedures to gain specific sample fractions are extensively described by Jackson [35], while Brindley
249 and Brown [7] or Moore and Reynolds [8] provide comprehensive instructions for routine analysis.
250 The US Geological Survey describes the different sample preparation techniques in an illustrated
251 laboratory manual [36]. Regarding the aim of the sample preparation, a distinction has to be made
252 between oriented mounts of the clay-sized fraction for the qualitative analysis of the clay minerals
253 and a randomly oriented powder specimen of the bulk sample for quantitative analysis.

254 In order to retrieve a bulk powder, a representative clay sample has to be crushed and ground. There
255 are two requirements for the sample: a particle size below 20 μm (best 5- 10 μm [8]) and random
256 orientation [37]. To achieve the former, hand grinding is unsuitable in most cases, while dry grinding
257 in ball or disc mills can easily overgrind the clay particles. The best results are reported to be achieved
258 using a McCrone micronizing mill [8, 37]. Random orientation is another challenging task, as
259 phyllosilicates tend to arrange in (001)-direction. Even though preferred orientation can be reduced by
260 using a side- loading technique, perfect randomness can only be achieved by spray drying [38], which
261 is, however, no commonly available laboratory technique.

262 Particle-size separation is usually required to obtain the pure clay-sized fraction. Grinding in advance
263 should be avoided, as thereby the clay-sized fraction gets enriched by non-clay minerals [39]. The
264 disaggregation procedure strongly depends on the host rock. For a successful fractionation, the clay
265 minerals need to be liberated while coagulation has to be prevented [40]. This can be achieved by
266 dispersing the suspended sample with a small amount (< 0.5 wt% [36]) of dispersant (e.g. sodium
267 pyrophosphate [8]) using an ultrasonic probe. Chemical treatments may be necessary, in order to
268 remove organics, carbonates, sulfates or iron oxides [35]. The XRD analysis of smectite rich clays is
269 influenced by the type of interlayer cation and can thus require homo-ionic exchange. This can be

270 achieved by treating the clay with a chloride solution of the corresponding cation, for example Li-
271 exchange is used to distinguish montmorillonite from other smectites [40]. Size fractionation is carried
272 out according to Stoke's law, using the different settling times depending on the particle size, which
273 is calculated as equivalent spherical radius. The procedure can be accelerated by centrifugation. While
274 the < 2 µm fraction is commonly used to prepare the oriented mounts, also the < 0.2 µm fraction can
275 be of interest in some cases, for instance to distinguish illite-smectite mixed layers (see 3.2.2).

276 The clay- sized dispersions are afterwards transferred to oriented mounts and measured in air- dried
277 condition. The easiest approach is to drip the suspension on a glass slide and let it dry. More
278 sophisticated methods, which improve diffraction intensities, are found in the literature [8].
279 Treatment of the oriented mounts in an ethylene glycol (EG) saturated atmosphere at 60 °C allows the
280 differentiation of swellable 2:1 clay minerals, as the *d*- values of the (001)- reflections increase with EG
281 solvation. A heat treatment of the mount at 550 °C helps to differentiate between kaolinite and
282 chlorite [8].

283 Data collection by laboratory powder diffractometers should be performed over a wide enough
284 angular range starting preferably at low angles in order to cover the typically high *d*-values for clay
285 minerals. High peak-to-background ratio as well as sufficient counting statistics should be aimed for,
286 in order to ensure proper data processing.

287 **3.2.2. Qualitative analysis**

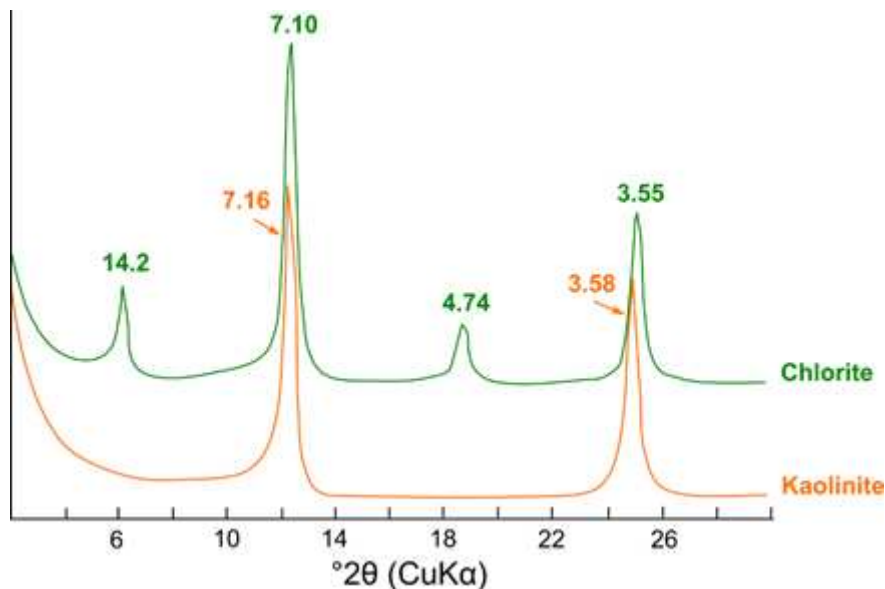
288 The goal of qualitative XRD analysis is to correctly identify all minerals present. This list of identified
289 minerals is the starting point for the next step of quantitative analysis, the more detailed the
290 identification, the more accurate the quantification result.

291 As whole-rock mineral quantification is usually the goal, qualitative analysis usually starts on XRD
292 measurements of the randomly oriented bulk sample [11]. Both non-clay and clay minerals can be
293 identified based on routine peak searching and matching analyses with supplied databases (e.g.
294 JCPDS) in common XRD analysis software. As an aid in identification Annex I gives a search list
295 containing *d*-values of the strongest reflection lines of common clay minerals and associated phases.
296 Due to significant peak overlap and unpredictable effects of preferred orientation, identification of
297 clay minerals down to the individual mineral species is usually not possible. Instead, aggregated groups
298 of clay minerals are usually distinguished, such as kaolins, comprising kaolinite, dickite, nacrite and
299 halloysite, or dioctahedral Al-rich 2:1 clays and micas, including illite, smectite, mixed-layer illite-
300 smectite, muscovite and pyrophyllite. In consequence, also the quantification is aggregated at the
301 same group level. While this level of detail may be sufficient to obtain total contents of kaolins, no
302 distinction is made between e.g. illite or smectite that are known to have a very different impact on
303 material performance as SCM. In addition, confusion may result from peak overlap, for instance
304 distinguishing kaolinite and chlorite is not straightforward (see Figure 1). The lack of detailed clay
305 analysis results in important knowledge gaps as regards the potential use as SCM of ubiquitous clay
306 minerals such as mixed-layer illite-smectite.

307 Detailed analysis of a sample's clay mineralogy is conveniently made by XRD measurements of
308 oriented aggregates of the < 2 µm and/or < 0.2 µm fraction. The orientation treatment strongly
309 enhances the (001) basal reflections of the clay minerals. Sampling the clay size fraction removes non-
310 clay minerals present in the sample to a large extent, as such simplifying further analysis. Regular,
311 discrete clay minerals can be identified by their rational series of (001) peaks, interspaced at regular
312 2θ intervals. Clay mineral peaks are characteristically broader than common non-clay minerals such
313 as quartz or feldspars. Distinguishing the main clay mineral types on oriented mounts is
314 straightforward. Kaolinite is recognized from its 7.16 Å and higher order reflections, illite from its 10
315 Å and higher order reflections, chlorite from its 14 Å and higher order reflections etc. (Figure 1 and

316 Figure 2). However, difficulties arise when peak overlap between different clay minerals occurs such
317 as between chlorite and kaolinite (Figure 1), or when mixed-layer clay minerals are present. To resolve
318 this issue, additional treatments are applied to the oriented sections. For instance, kaolinite and
319 chlorite can be distinguished by a heat treatment of 1 h at 550 °C, at which temperature kaolinite will
320 be decomposed while swelling clays potentially obscuring the 14 Å chlorite (001) peak will be collapsed
321 to 10 Å and the chlorite 14 Å peak will become better visible. Swelling clays, such as smectites, are
322 more easily identified after ethylene glycol (EG) solvation treatment. As illustrated in Figure 2 the main
323 peak of smectite (in its Ca-form) shifts from 14-15 Å in the air-dried state to about 17 Å when solvated
324 by EG treatment, non-swelling clays such as illite or chlorite are not affected by EG solvation.

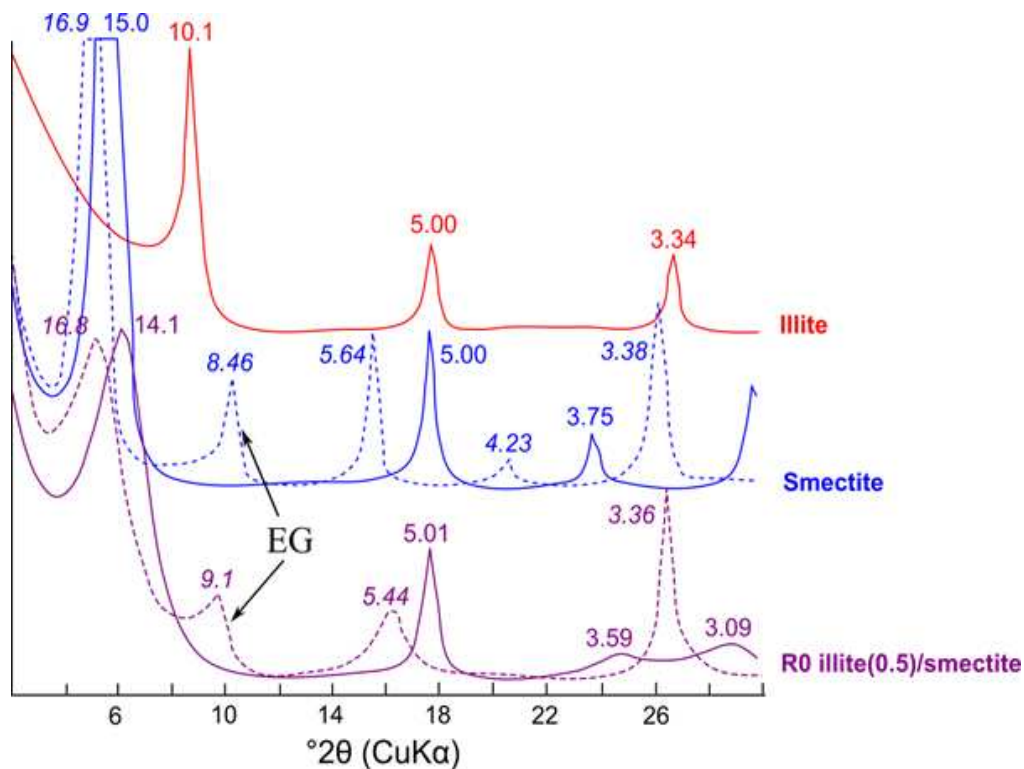
325 Additional information can be gained from examining the (060) reflection in the randomly oriented
326 bulk sample. The *b* lattice parameter is sensitive to the cation size and site occupancy in the octahedral
327 sheet and is therefore useful to distinguish between di- and tri-octahedral clay types. Di-octahedral,
328 Al-rich clay minerals such as kaolinite, montmorillonite and illite have (060) reflections from 1.490 to
329 1.499 Å. Tri-octahedral Mg-rich clay minerals such as biotite, chlorites or palygorskite have (060)
330 reflections in the range of 1.530 to 1.560 Å (cf. Annex I).



331

332 *Figure 1. XRD patterns of oriented mounts of chlorite and kaolinite illustrating strong overlap of the*
333 *(001) reflections.*

334 Mixed-layer clay minerals can be recognized by irrationally spaced or aperiodic reflection series and
335 variable (001) peak widths (Figure 2). Both peak positions and width are used to estimate the sequence
336 and proportioning of the interlayered clay minerals by applying the Méring principle [41]. For instance
337 in Figure 2 the proportioning 50/50 between illite and smectite can be derived from the difference in
338 peak position between the 001/002 (peak at 9.1 Å) and the 002/003 (peak at 5.44 Å) peaks of the EG
339 solvated sample.



340

341 *Figure 2. XRD patterns of oriented mounts of illite, smectite and mixed-layer R0 illite(0.5)/smectite, the*
 342 *shift in basal reflections of the smectite clay minerals by ethylene glycol (EG) solvation is illustrated.*

343

344 3.2.3. Quantitative analysis

345 Quantitative phase analysis (QPA) of raw clays by XRD is challenging because of the wide variety in
 346 chemical composition and crystalline structures, the occurrence of structural disorder such as
 347 interlayering or stacking disorder, and potential presence of amorphous phases [7, 11, 42].

348 QPA methods can be grouped in two categories: the first category includes those techniques aimed at
 349 quantifying the fraction of a given phase within a mixture, based on the intensity of a single reflection
 350 within the XRD pattern. The second category comprises *whole pattern methods*, by which
 351 quantification is achieved by fitting the full diffraction pattern.

352

353 Single reflection methods based on the addition of standards (internal standard methods) rely on
 354 removing the unknown mixture linear X-ray absorption coefficient from the equation that expresses
 355 the measured intensity of a given peak, relative to a given phase, to the volume fraction of that phase
 356 in the mixture [43]. The fraction of a crystalline phase within a mixture can be quantified by comparing
 357 the intensity of a selected reflection with that of a reflection of a standard phase. This phase can be
 358 added in known amount to the sample as internal standard, or separately measured as external
 359 standard. Internal standards should have low attenuation coefficients and few XRD reflections,
 360 possibly not overlapping with those of the phase to be quantified [7]. Care should be taken in
 361 homogeneously intermixing the sample with the standard. Typically, levels of 10 or 20 wt.% of internal
 362 standard are used, however higher levels may be preferable in certain cases. Common standard
 363 materials are corundum ($\alpha\text{-Al}_2\text{O}_3$) and zincite (ZnO). Different versions of the internal standard method
 364 exist, mainly differing in the standard and the reference reflections of choice [44]. For example, the
 365 (113) reflection in corundum is used in the Reference Intensity Ratio (RIR) method [45]. In the external
 366 standard method, difference in the linear X-ray absorption coefficients of the sample and standard
 367 are mathematically accounted for, relying on accurate determinations of the sample and standard
 368 chemistry [46].

369

370 Single reflection methods often struggle with complex multicomponent materials that show broad
371 and overlapping peaks, such as clays. Clay mineral peaks are often quite variable in peak width and
372 intensity due to variations in microtexture, chemical composition and structure. Therefore, it is
373 important to make calculations based on integrated peak intensities (peak area), rather than peak
374 heights [47]. In addition, clay mineral reflections are often prone to preferred orientation (e.g. the 00/
375 peaks). Such reflections should be avoided for accurate and reliable quantification. Single line
376 reflections that are less sensitive to preferred orientation or variations in chemistry and structure,
377 such as the above-mentioned (060) reflections for clay minerals, therefore need to be identified and
378 calibrated for quantification purposes. The accuracy of single reflection methods can suffer
379 significantly from peak overlap issues. This can be, to some extent, resolved by computationally fitting
380 the whole observed pattern.

381

382 When it comes to whole pattern analysis, again two approaches are distinguished. In one approach,
383 designated as “full pattern summation”, the pattern is fitted by combining measurements of pure
384 reference minerals that are pre-recorded on the same XRD instrument [48]. The scaling factors for
385 each mineral are then recalculated to mass fractions using pre-determined conversion factors, in
386 similar ways as for single-line reflections [10]. The advantage of full pattern summation methods is
387 that there is no need to know the crystal structure of the clay mineral of interest. This can be
388 advantageous in case of highly variable and defective clay structures such as mixed-layer clay minerals
389 or smectites. The disadvantage is that pure or at least simple mixes of the mineral phase of interest
390 need to be available and pre-recorded for each lab instrument that is used. It is important to note that
391 the accuracy of this approach strongly depends on the selection and availability of appropriate mineral
392 standards [10, 49]. Examples of software packages implementing the full pattern summation approach
393 for clay analysis include FULLPAT [50], QUANTA® [51], RockJock [52], and PowdR [53, 54].

394 In the alternative approach, the pattern is fitted by theoretically calculated diffraction patterns using
395 crystal structural and textural data in the Rietveld method. Rietveld quantification has as advantage
396 that there is no need for building a library of pure reference patterns as diffraction patterns are
397 calculated directly from crystallographic data and the diffractometer geometry [55]. The main
398 drawback of Rietveld based methods is that they typically assume three dimensional periodicity, which
399 is often not the case for clay minerals that show complex interstratification and defect crystal
400 structures leading to strongly asymmetric peaks [56]. Specific software or software having extensions
401 capable of dealing with interstratified clay minerals include Profex/Autoquan/BGMN [57, 58], and
402 TOPAS/TOPAS-Academic [59, 60]. As these extensions may be somewhat computationally expensive,
403 also hybrid approaches combining Rietveld for known, crystalline phases, with profile summation for
404 Partially Or Not Known Crystal Structures (PONKCS) have been developed and successfully applied to
405 quantitative XRD analysis of clays [61].

406

407 In the internal and external standard methods, the amorphous phase content is calculated as the
408 difference between the sum of all crystalline phase mass fractions and 1. This fraction may also include
409 contributions from non-identified minerals and misfits of the calibrated patterns or crystal structures
410 and is therefore often referred to as “unknown and amorphous phase” fraction [62].

411

412 **3.3. Thermal analysis**

413 Thermal analysis is a general term that covers a variety of techniques that record physical and chemical
414 changes occurring in a substance once it is subjected to changes in temperature. Four of these
415 techniques, Thermogravimetric Analysis (TGA), Differential Thermal Analysis (DTA), Differential
416 Scanning Calorimetry (DSC) and Loss on Ignition (LOI) have become powerful tools for qualitative and
417 quantitative analysis of clays and clay minerals [63, 64]. In fact, clays were among the first materials

418 investigated by thermal analysis, following the early development of these techniques at the end of
419 the 19th century [65].

420

421 The International Confederation of Thermal Analysis (ICTA) defines DTA as a method that monitors
422 the temperature difference between a sample and a thermally inert reference as a function of time
423 and/or temperature. DTA therefore allows to detect exothermic and endothermic phenomena. A
424 similar technique, DSC, records the energy associated to the exothermic or endothermic phenomena
425 by applying and measuring power compensation to equalize temperatures or by measuring the heat
426 flux between the sample and the reference. For quantitative analysis, DSC is by principle superior to
427 DTA since the former method not only registers the endothermic/exothermic effect but also allows
428 direct measurement of its associated energy. However, the achievable upper temperature limit in DSC
429 is often lower than that of DTA [66]. In contrast, TGA measures the change in mass of a material over
430 a temperature range using a predetermined heating rate or as a function of time under an isothermal
431 regime. This technique is very useful for monitoring phenomena associated to mass changes, such as
432 decarbonation, dehydration, dehydroxylation, decomposition of sulfides/sulfates, combustion and
433 oxidation reactions. By performing stoichiometric calculations, the registered mass changes can be
434 used for quantitative purposes [67, 68].

435

436 Combination of TGA with DTA/DSC is increasingly available in modern thermal analysis instruments.
437 In this combined analysis a temperature shift is usually observed between TGA and DTA/DSC curves
438 for the same phenomena. This is because mass changes are detected almost instantaneously while
439 the associated temperature changes are perceived with some time delay by DSC. The magnitude of
440 this shift is dependent on experimental factors such as heating rate or the amount of analyzed sample.
441 The best sample arrangement for TGA experiments is a thin layer of powdered sample that allows a
442 swift release of decomposition gases, whereas the best one for DTA is the sample totally surrounding
443 the thermocouple, to increase the efficiency of the thermal signal. Slow heating rates may favor
444 resolution in TGA curves but decrease the intensity of the signal detected by DTA/DSC [63, 67, 69]. As
445 both measurements cannot be made in their optimal configuration at the same time, compromise
446 solutions are often used. Traditional thermal analysis techniques may also be complemented by
447 evolved gas analysis methods (EGA), that through the use of FTIR, gas chromatography or mass
448 spectrometry assist in the interpretation of the nature and the amount of the evolved products for a
449 given reaction, such as H₂O, CO₂ or SO₂ [69].

450

451 **3.3.1. Qualitative thermal analysis of clays**

452 Upon heating of raw clays from room temperature to approximately 1000 °C, three phenomena can
453 be clearly distinguish in thermal analysis curves: i) dehydration (~50-300 °C, mass loss, endothermic),
454 ii) dehydroxylation (~350-950 °C, mass loss, endothermic) and iii) recrystallization (for temperatures
455 >900 °C, exothermic, no mass changes, only detected by DSC/DTA). While DTA/DSC are always
456 represented as differential curves, where clearly visible peaks can be directly associated to the
457 occurring transformations, TGA is depicted as a step-like curve, with a much lower resolution between
458 consecutive thermal phenomena. Therefore, for accurate qualitative interpretation of TGA curves the
459 use of the first derivative of the thermogravimetric curve (DTG) is strongly advised, which allows not
460 only to improve resolution between adjacent thermal phenomena but also to detect small mass
461 changes that may not be directly spotted from the regular thermogravimetric curve [68, 70].

462

463 Dehydration is the release of molecular water that may be adsorbed at the inner/outer surface of
464 minerals or trapped within its pore or channel structure. Molecular water is also present in the
465 interlayer region of most 2:1 clay minerals, associated to the cations positioned in the interlayer. For
466 clay minerals, the magnitude and temperature range of the dehydration step depends on a large
467 number of factors such as storage conditions, structure and crystallinity of the clay mineral, and nature

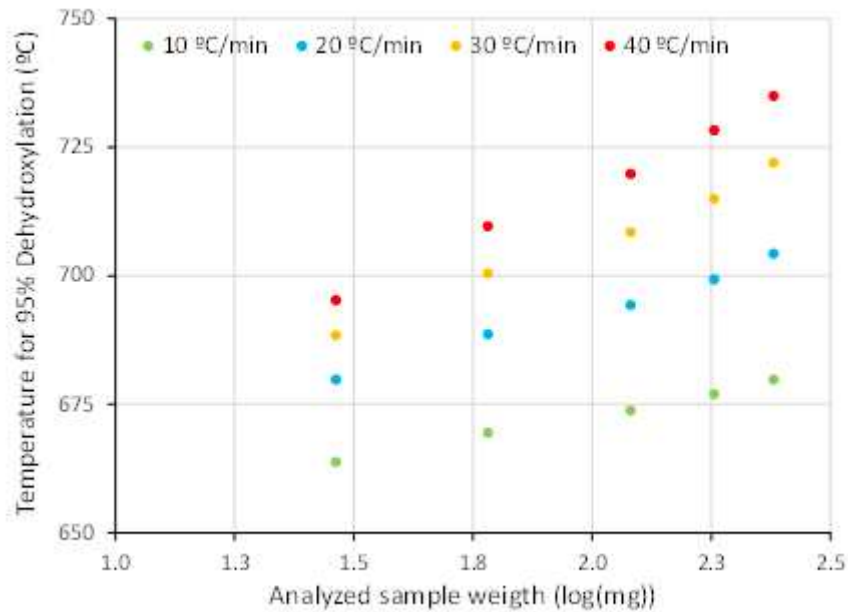
468 and abundance of the cations in the interlayer region, among others [71, 72]. Dehydration is
469 particularly useful to identify the presence of 2:1 clay minerals that exhibit strong dehydration effects,
470 such as smectites, vermiculites or some micas, with typical mass losses that range from 7 to 17 wt. %
471 in air dried samples [63, 68, 69]. However, it should be stress out that not only 2:1 clay minerals may
472 exhibit significant dehydration steps, as this is also the case for halloysite (~12 wt. %), poorly
473 crystallized kaolinites and some non-crystalline associated phases to 1:1 clay minerals, such as
474 allophane and imogolite [67, 68].

475

476 The hydroxyls groups in the clay structure are much more strongly bonded than adsorbed or interlayer
477 water and requires a higher temperature for its removal. Upon heating, hydroxyls are liberated over
478 a broad temperature range related to their different locations within the clay mineral structure and
479 their wide range in bond energy distribution. As a general rule, clay minerals with a higher level of
480 structural disorder exhibit dehydroxylation effects at lower temperatures and within a wider
481 temperature range compared to the same clay minerals with a higher crystallinity [71, 73, 74]. The
482 nature of the cation bonded to the hydroxyl group also influences dehydroxylation temperature, as
483 the bond energy increases according to the sequence Fe-OH < Al-OH < Mg-OH [63, 64]. The mass
484 fraction that hydroxyls represent in the structural unit, their position in the crystal lattice as well as
485 their average bond energy are characteristic to each individual clay mineral. Therefore, the
486 temperature range, peak temperature, shape, and magnitude of the thermal effects associated to the
487 dehydroxylation of clay minerals are of great analytical value for both qualitative and quantitative
488 interpretation of clay samples.

489

490 Concerning sample characteristics, the temperature range and rate of dehydroxylation is mainly
491 depending on the degree of structural disorder of the clay minerals, the size distribution of crystallites
492 and physical particles, and the degree of packing [71, 73-75]. Due to heat diffusion effects, an increase
493 in sample size or in heating rate will shift dehydroxylation temperatures to higher values, following a
494 logarithmic law as observed in Figure 3 for a natural kaolinite. In order to keep results comparable,
495 linear heating rates of 10 °C/min and analysed sample masses of about 30-50 mg are usually
496 recommended as experimental conditions in most modern equipment. As for furnace atmosphere or
497 purge gas, air is the usual option, in case carbonation of oxidation needs to be avoided an inert
498 atmosphere (nitrogen, argon) is preferable. Given the strong influence that experimental conditions
499 and sample characteristics have on the dehydroxylation temperature range, there is a large scatter of
500 temperature values reported in the scientific literature for similar clay minerals. An attempt is given
501 in Table 1 to summarize the behaviour of selected clay minerals relevant as source of SCM. As noticed,
502 although dehydroxylation may occur over a wide range of temperatures (grey temperature ranges in
503 Table 2), for each group of clay minerals there is a relatively narrow temperature interval (black
504 temperature ranges in Table 1) in which most of the dehydroxylation phenomena (>90%) take place.



505

506 *Figure 3. Influence of heating rate and sample mass in dehydroxylation temperature of a kaolinite*
 507 *sample*

508 *Table 1. Temperature ranges for dehydroxylation of some representative clay minerals, data adapted*
 509 *from [63, 68]*

	ΔOH^- (wt.%)	Clay mineral	Dehydroxylation temperature (°C)							
			300	400	500	600	700	800	900	1000
Kaolinite group	~ 14.0	Kaolinite	300-400	400-600	600-700	700-800				
		Dickite	400-500	500-700	700-800	800-900				
Smectite group	4.3 - 5.0	Nontronite	300-400	400-600	600-700	700-800	800-900			
		Montmorillonite	300-400	400-500	500-600	600-700	700-800	800-900		
True and brittle micas	4.5 – 5.3	Muscovite	300-400	400-600	600-700	700-800	800-900	900-1000		
		Illite	300-400	400-500	500-600	600-700	700-800	800-900	900-1000	

510

511 Finally, at temperatures above 900 °C, recrystallization takes place, indicating the conversion of
 512 structurally disordered, metastable phases to more stable, crystalline high-temperature phases.
 513 Common phases formed during recrystallization are mullite, cordierite, enstatite and cristobalite.
 514 Similar to dehydroxylation, the temperature, width and shape of the exothermic recrystallization peak
 515 depends on the type, crystallinity and amount of clay minerals present in the sample [63, 67, 76].
 516 Identification of these three temperature ranges are amongst the most useful information (and easily
 517 obtained) for a potential SCM, as they inform the feasible range of calcination temperature for a given
 518 clay. Alongside the clay minerals themselves, TG curves can also be helpful in identifying associated
 519 minerals in clays and soils - particularly those which diffract weakly in XRD patterns (due to poor
 520 crystallinity and/or fine particle size) but exhibit distinctive mass loss behaviour, such as goethite [77].

521 3.3.2. Quantitative analysis of clays based on TGA/DTG curves

522 Quantitative analysis by TGA is based on the assumptions that, within a given temperature range, an
 523 individual mineral is solely responsible for the registered mass changes, that the registered reaction
 524 follows a known stoichiometry, and that chemical variability for the quantified mineral is low enough
 525 so that precise calculations based on the registered mass changes are possible. The accuracy is

526 favoured for phases with a lower stoichiometric factor, i.e. with a lower ratio between its molar mass
527 and the mass change associated to its decomposition reaction. Therefore, the accuracy of quantitative
528 analysis based on TGA measurements is different for each mineral [63]. An important potential source
529 of error is the overlap between decomposition reactions of the different clay and non-clay minerals
530 present in the sample. In a best case scenario this only decreases the accuracy of the determination,
531 however in unfavourable conditions this may totally obstruct the identification and quantification of
532 individual minerals [68]. Finally, all quantitative results should be reported based on dry mass and not
533 initial sample mass. Variable amounts of absorbed/adsorbed water in clay samples should not be
534 taken into account in stoichiometric calculations.
535 The expression used to calculate the quantity of a given clay mineral based on its dehydroxylation
536 reaction is:

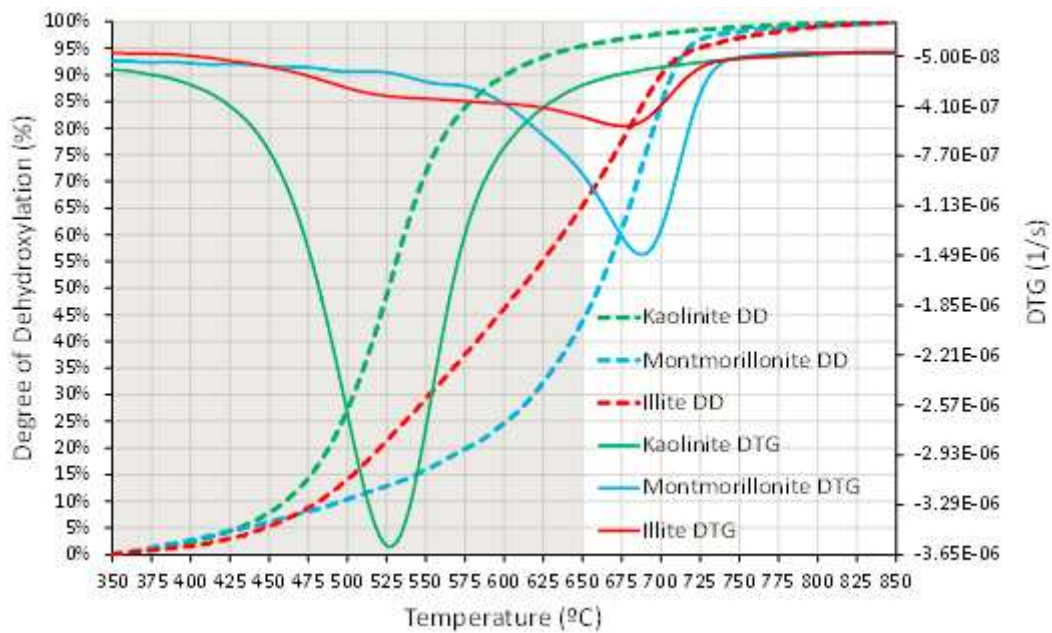
$$537 \quad \text{Clay mineral content} = \frac{100 * (\text{Mass}_{T1} - \text{Mass}_{T2})}{\text{Mass}_{\text{Dry}} * \Delta\text{OH}} \quad \text{Eq 1}$$

538 In Equation 1 the difference (Mass T1 - Mass T2) represents the mass loss over the dehydroxylation
539 interval, with T1 and T2 being the lower and upper temperatures of the interval. Mass_{Dry} is the mass
540 of the dry sample (usually at temperatures between 200 -250 °C); while ΔOH is the mass fraction of
541 the clay mineral represented by hydroxyl groups, without considering the variable content of
542 absorbed/adsorbed water in the stoichiometric calculations. The value of ΔOH , expressed as mass
543 percent, is ~14 wt. % for 1:1 clay minerals and range from 4 to 5.5 wt. % for 2:1 clay minerals that
544 show larger chemical and structural variability [78]. Different approaches can be followed to
545 determine the mass loss associated to a given thermal phenomenon, the two most common being the
546 tangent method in the TGA curve and the peak integration method in the DTG curve. Combined
547 analysis is also quite suitable, by using the DTG curve to select temperature limits for the
548 dehydroxylation effect and then calculating mass changes in the TGA curve using the previously
549 defined temperature interval [69].

550 Although quantitative analysis by TGA is possible for all individual clay minerals, for complex
551 mineralogical systems reliable quantification is mainly limited to members of the kaolinite group,
552 characterized by a low variability in its chemical composition and a lower stoichiometric factor (~7.2)
553 in comparison to 2:1 clay minerals (~19-23). Whilst quantitative analysis for clay minerals with variable
554 composition can be attempted, this requires either an assumption of the stoichiometric formula [79]
555 which reduces accuracy, or labour-intensive laboratory work to determine the exact formula of the
556 clay mineral of interest (which is arguably not worth the effort involved). Some degree of overlap
557 cannot be avoided between kaolinite dehydroxylation and decomposition of 2:1 clays or some non-
558 clay minerals such as pyrite, alunite or poorly crystallized carbonates, all mineral phases that can be
559 found naturally associated to kaolinite [74, 75]. Therefore, before starting qualitative or quantitative
560 interpretation of thermal analysis, the gathering of additional information regarding the mineralogical
561 composition of the analysed sample is strongly advised, either by using other characterization
562 techniques such as XRD and FTIR; or by collecting information from literature. The identification of
563 minerals that may overlap with the thermal dehydroxylation of clay minerals is of obvious importance.
564 Once this is done, measurement bias can be minimized by carefully selecting the temperature range
565 for determination of mass losses on the DTG curve, or by using a slower heating rate (yielding a higher
566 sensitivity and a better resolution) to detect and distinguish smaller mass change events.

567 The above statements are illustrated in Figure 4, where DTG curves for representative members of
568 clay mineral groups commonly used as or associated to SCM source materials are shown together with
569 the characteristic S-shaped curves that describe the degree of dehydroxylation under a linear heating
570 rate of 10 °C/min. As can be observed, although dehydroxylation of kaolinite covers approximately
571 the entire range between 350 to 800 °C, for practical purposes the upper limit for determining mass
572 losses could be set to 650 °C, a temperature for which kaolinite has reached 95% degree of
573 dehydroxylation and the overlap with the dehydroxylation of illite and montmorillonite is kept to a
574 minimum. Finally, it should be stressed that in complex mineral mixtures it is almost impossible to

575 distinguish by thermal analysis measurements between the different clay minerals of the kaolinite
576 group, making it more correct to group results as a single value, denoted as equivalent kaolinite [80].
577 Similar reasoning also applies to complex mixtures of 2:1 minerals.



578

579 *Figure 4. Degree of dehydroxylation and DTG curves for kaolinite, montmorillonite and illite (heating*
580 *rate 10 °C/min). Temperature limits selected for (equivalent) kaolinite quantification are indicated by*
581 *the shadowed area.*

582 Because the above-mentioned phenomena may interfere to some extent with accurate
583 determinations of clay minerals by TGA/DTG, it is always advisable to cross-check quantitative results
584 obtained by thermal analysis with other analytical techniques. In general, good agreement has been
585 reported when comparing XRD with TGA results for kaolinite group minerals, as depicted in Figure 7,
586 however there are few reports for 2:1 clay minerals. Major differences are expected for samples with
587 low crystallinity, because clay minerals may be underestimated by XRD, while the trend in TGA may
588 show a slight overestimation due to overlapping of thermal decomposition events of other minerals.
589 The chemical composition could be used to double check results from mineralogical analysis,
590 especially for clay minerals with a low chemical variability. For example, for any given sample, kaolinite
591 content should always be lower than the mass ratio $Al_2O_3/0.395$, corresponding to the chemical
592 composition of kaolinite clay minerals [13].

593

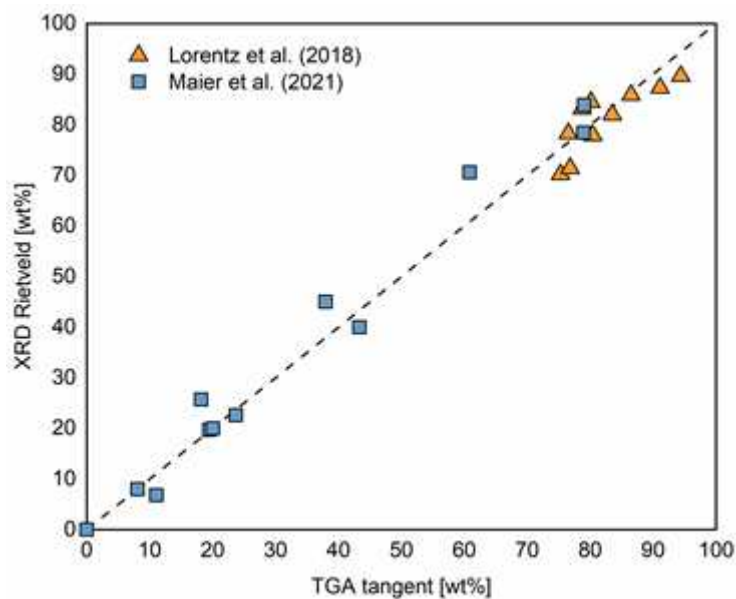


Figure 5. Comparison of kaolinite content determined by XRD and TGA, data from [13, 19].

3.3.3. Loss on Ignition

Loss on ignition (LOI) measurements are a well-known technique in the study of soils and minerals and also a useful way to characterise raw clays. The concept is similar to that of TGA except that the mass loss measurements are intermittent instead of continuous. LOI measurements are usually conducted by placing a few grams of crushed or powdered material in a muffle furnace at set temperatures (e.g., 200°C, 550°C, 950°C, 1050°C) and the mass loss recorded over each interval. LOI measurement has the advantage over TGA in that it does not require sophisticated equipment and is quite straightforward to be carried out. Another major difference between LOI and TGA is that there is less control of the atmosphere for LOI measurements as these are usually done without a purge gas. LOI can be a valuable indicator for the presence of certain minerals as well as to test the variability/consistency of the raw clays. LOI tests may be used for quality control of clay – for example, ASTM C311/C311 M – 13 instructs for natural pozzolans (including calcined clays) to be ‘ignited to constant mass’ at 750 ± 50 °C, with a maximum allowable LOI of 10%. For kaolinitic clays, the kaolinite content may be estimated from the mass difference recorded after heating to 400 and 600°C [81]. However, such tests may also fail to provide correct assessment in case more than one mineral loses mass over the targeted temperature range [81]; for example, calcite [82], which can be found in soils.

3.4. Vibrational spectroscopy

3.4.1. Infrared spectroscopy

Infrared spectroscopy was introduced in the middle of the 20th century to study the bond structures of solid, liquid, and gaseous molecules. IR spectroscopy involves measuring the resonance between IR photons and the vibrational energy of molecular bonds [83], and the instrumentation is commonly used in three subranges: near- (12,500–4000 cm⁻¹), mid- (4000–400 cm⁻¹), and far-IR (400–10 cm⁻¹). When infrared radiation is sent through the sample part of the energy spectrum is absorbed to cause the excitation (stretching, rotation, and bending) of specific bonds in the molecules. The frequency, intensity, and width of the absorbance signal obtained depend on the sample's local structure, composition, and microstructure. Every molecule has a unique IR fingerprint, making IR-spectroscopy an invaluable technique to identify minerals, especially in clay science [84].

MIR for clay minerals identification

625 In this section, the focus is on the interpretation of mid infrared (MIR) absorbance spectra for clay
626 characterization. In this case, sample preparation requires careful intergrinding of 1 wt.% of raw clay
627 with KBr powder² to avoid crystalline alteration. The resulting powder is subsequently pelletized under
628 load. The pellet can be kept in an oven at 105 °C for extended periods to avoid or remove absorbed
629 moisture. A standardized procedure for pellet preparation is critical for obtaining consistent and
630 comparable FTIR spectra for clay identification [85].

631

632 For clay minerals, the characteristic absorption bands present in the MIR range (4000–400 cm⁻¹) are
633 associated mainly with stretching and bending vibrations O-H and Si-O bonds, and Al-O, Fe-O and Mg-
634 O bonds. According to the clay mineral structure (OH groups coordinated with octahedral atoms, the
635 interlayers cations, surrounding tetrahedral lattice), the absorbed energies at different wavenumber
636 have a typical molecular spectrum. A recent review of IR-spectra of clay minerals is published by
637 Madejová et al. [86]. The main bands for identification clay minerals in common clays are listed in
638 Annex II. Whilst MIR spectroscopy is predominantly a laboratory-based technique, portable handheld
639 instruments have now entered the market – a previous study has shown comparable performance to
640 desktop instruments in the characterisation of soils [87]. Such advances in instrumentation could help
641 open up MIR spectroscopy as a rapid, on-site technique for clay prospecting.

642

643 **1:1 clay minerals - kaolins**

644 Figure 6 shows the FTIR spectra of 1:1 clay obtained from Madejova et al. [86] as an example. In the
645 OH stretching region (3600 – 3700 cm⁻¹), ordered kaolinite (Figure 6a) shows four bands at 3694, 3669,
646 3652, and 3620 cm⁻¹ [88-91]. The 3620 cm⁻¹ band is attributed to the stretching vibrations of inner OH-
647 bonded to octahedral cations, and the other bands are due to coupled stretching vibrations of OH
648 groups located at the surface of the dioctahedral sheet of the layers. The 3694 cm⁻¹ band corresponds
649 to the in-phase coupled stretching vibration of surface-perpendicular-OH, whereas the 3669 and 3652
650 cm⁻¹ bands are due to out-of-phase coupled vibrations of these groups [88, 89]. For disordered
651 kaolinite (Figure 6b), the bands at 3620 and 3694 cm⁻¹ remain, while a single band replaces the doublet
652 of 3669 and 3652 cm⁻¹ at 3653 cm⁻¹ [92]. The PO index measures the crystallinity, which is calculated
653 as the intensity ratio of the bands at 3620 cm⁻¹ and 3694 cm⁻¹ [91]. PO > 1 reveals an ordered structure,
654 and PO < 1 indicates a disordered structure. The PO index can be affected by the presence of illite,
655 quartz, or feldspars [92].

656

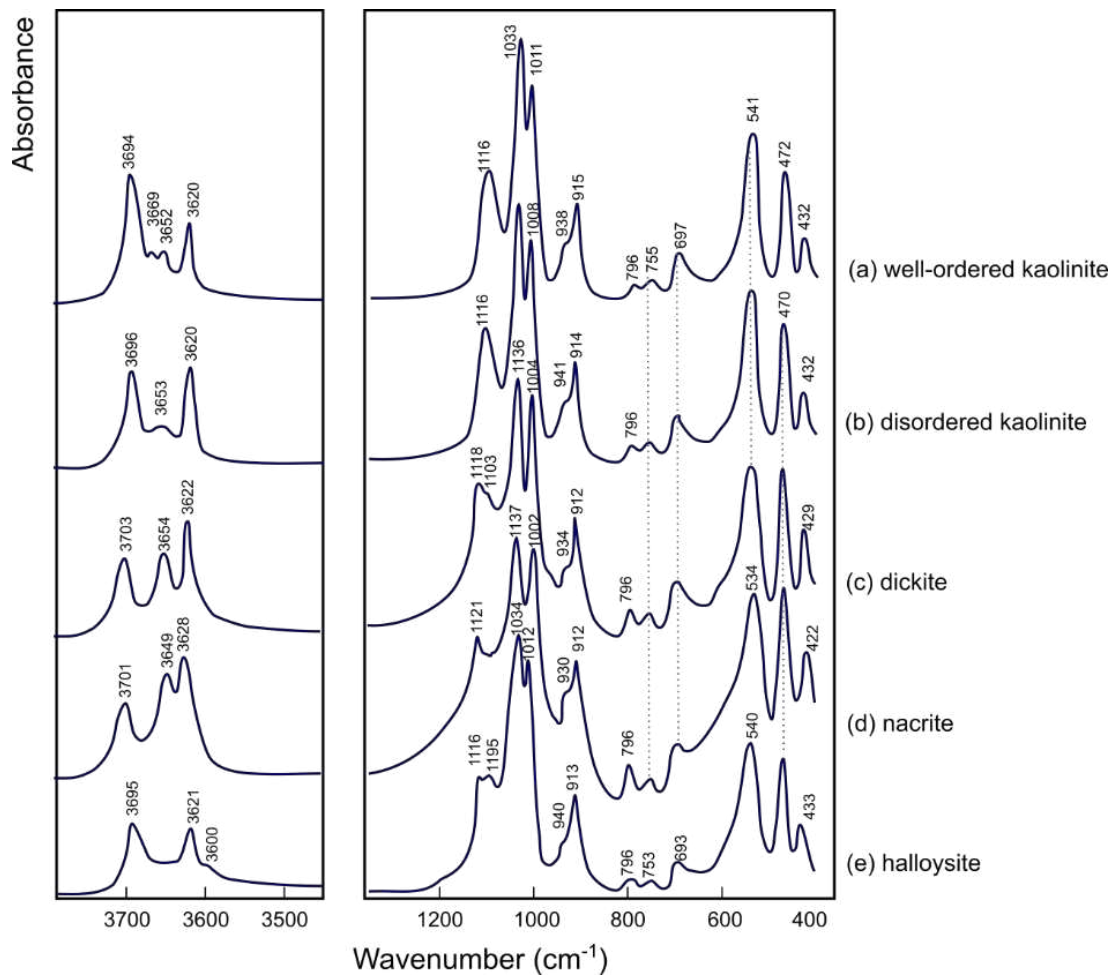
657 In the OH- regions, the dickite spectrum shows three absorption bands at 3703, 3654, and 3622 cm⁻¹
658 (Figure 6c) (Balan et al., 2010). The 3623 cm⁻¹ band is assigned to the inner OH, the 3710 cm⁻¹ band to
659 the inner-surface OH, and the 3656 cm⁻¹ band to the remaining OH groups. Nacrite (Figure 6d) shows
660 similar OH- stretching bands to those of dickite in this region. Halloysite (Figure 6e) shows two
661 prominent bands at 3695 cm⁻¹ and 3621 cm⁻¹ in the OH stretching region, while two weak intermediate
662 bands could be found in prismatic tubular halloysite [93].

663

664 In the 1400–400 cm⁻¹ region (Figure 6), the spectra of 1:1 kaolin-group clay minerals are similar,
665 showing a strong and sharp band in the 1120–1000 cm⁻¹ region assigned to the Si-O stretching
666 vibrations, two strong bands at 1037–1033 cm⁻¹ and 1012–1002 cm⁻¹ attributed to the Si-O-Si
667 stretching vibrations, and around to 1100 cm⁻¹ due to Si-O bond stretching. At 470-472 cm⁻¹, the
668 bending vibrations Si-O-Si groups are displayed. Related to alumina bonds, the bending vibration of
669 Al₂OH bands appears near 915 and 935 cm⁻¹, the bending vibrations of Si-O-Al^{VI} near 540 cm⁻¹ [94].

670

² KBr is hygroscopic and should be dried and kept dry before measurement in order to avoid detecting diffuse water signals in the measurement.



671

672 *Figure 6. MIR spectra for 1:1 clay minerals: a) well-ordered kaolinite; b) disordered kaolinite; c) dickite;*
 673 *d) nacrite, and e) halloysite (adapted from [86]).*

674

675

676 **2:1 layer clay minerals: smectites, illite and muscovite**

677 The most common 2:1 layer-type clay minerals include smectites, illites, and micas. Smectites and
 678 micas are usually classified as dioctahedral and trioctahedral. In the smectite, the negative charge on
 679 the layers is balanced by hydrated exchangeable cations in the interlayer space or surface. On the
 680 contrary, no hydrated cation occupies the interlayer spaces in the illites and micas.

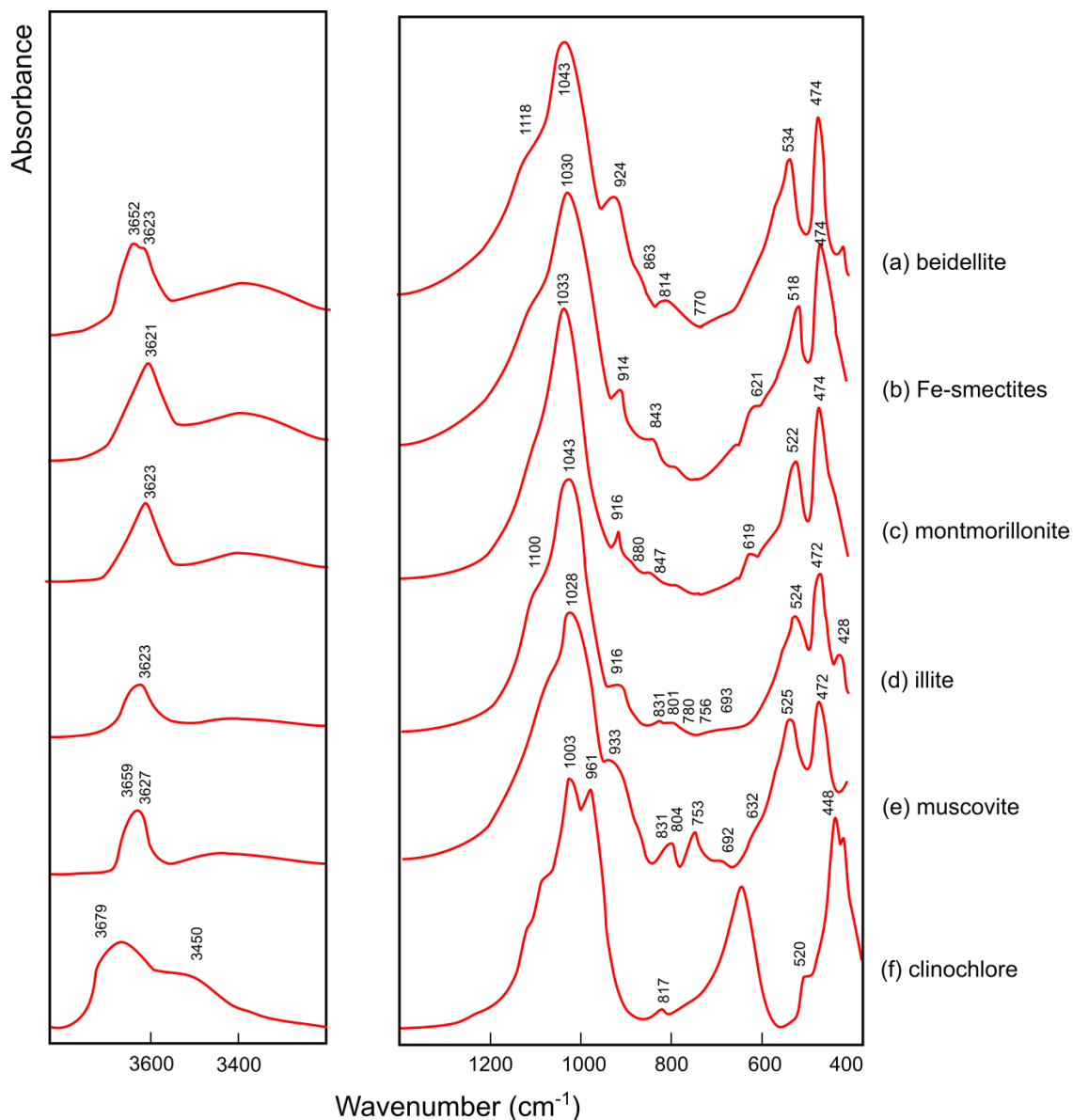
681

682 For smectites (Figure 7a to c), the OH- stretching region shows a broad band in the 3620–3650 cm⁻¹
 683 range assigned to the OH groups coordinated to different octahedral cations, mainly Al₂OH, AlMgOH,
 684 and AlFe³⁺OH. In smectites dominated by tetrahedral substitution (e.g. Si by Al in beidellite), the OH⁻
 685 bands appear at higher wavenumbers (3652 and 3623 cm⁻¹) than those dominated by octahedral
 686 substitution (e.g. Al by Mg in montmorillonite) with a band at 3623 cm⁻¹.

687

688 The OH bending region (950–800 cm⁻¹) is more sensitive to the occupancy of the octahedral sheets:
 689 the bands at 924 cm⁻¹ assigned to (Al₂OH) and at 863 cm⁻¹ assigned to AlMgOH are shown in the
 690 spectrum of beidellite (Figure 7a). For montmorillonite (Figure 7c), the band at 880 cm⁻¹ is assigned to
 691 AlFe³⁺OH. In the Si-O stretching region, smectites show a broad band assigned to Si-O-Si stretching
 692 vibrations (1070–970 cm⁻¹) and perpendicular Si-O vibration near 1100 cm⁻¹ [94].

693



694

695 *Figure 7. MIR spectra for layer minerals: a) beidellite, b) Fe-smectite; c) montmorillonite; d) illite and*
 696 *e) muscovite (selected and adapted from [86]).*

697

698 Figure 7d presents an IR spectrum of illite. In the OH stretching region, a single band is apparent at
 699 3623 cm⁻¹. In the 1400–400 cm⁻¹ region, the bands around 1043 cm⁻¹ are assigned to Si-O stretching
 700 vibrations. The (Al₂OH) band at 916 cm⁻¹ is similar to those found for montmorillonites. A weak band
 701 at 831 cm⁻¹ of illites is assigned to octahedral AlMgOH bending vibration or Al^{IV}-O vibration out of
 702 plane, and the 756 cm⁻¹ band to Al-O-Si vibration [94]. The 801 and 780 cm⁻¹ doublet is characteristic
 703 for quartz present in the sample.

704

705 For muscovite (Figure 7e), the spectrum shows OH stretching vibrations at 3627 cm⁻¹, a shoulder near
 706 3659 cm⁻¹ related to OH groups close to AlO₄ tetrahedron, and a band at 3627 cm⁻¹ assigned to OH
 707 groups bonded with neighbouring SiO₄ tetrahedra. The Si-O stretching and OH bending vibrations
 708 appear as broad bands (1028 and 933 cm⁻¹). Also, tetrahedral substitution generates bands at 831 and
 709 753 cm⁻¹ are attributed to the vibration of Al^{IV}-O and Al^{IV}-O-Si, respectively. The 524 cm⁻¹ band is due
 710 to Al^{VI}-O-Si bending vibrations, and both 472 and 428 cm⁻¹ bands are assigned to Si-O-Si bending
 711 vibrations.

712

713 **2:1:1 clay minerals: chlorites**

714 In case of chlorites the crystal structure is formed by a regular stacked 2:1 layers separated by a
715 brucite-like interlayer. FTIR spectra of chlorites include the stretching vibration bands of OH groups
716 from both the 2:1 layer and the hydroxide sheet that occupies the interlayer [92]. For example,
717 clinocllore (Figure 7f) shows a broad band at 3628 cm^{-1} with a weak inflection near 3680 cm^{-1} and a
718 wide shoulder centred near 3450 cm^{-1} . The bands at 3628 and 3450 cm^{-1} are assigned to the OH
719 stretching vibrations of the interlayer, and the absorption band near 3680 cm^{-1} is related to the Mg-
720 OH stretching vibration in the trioctahedral 2:1 layer [86]. In the Si-O stretching region, clinocllore
721 shows a splitting Si-O band (1003 and 961 cm^{-1}), and the band at 820 cm^{-1} is assigned to the Al-O
722 vibrations. The bands assigned to OH bending vibrations at $700\text{--}600\text{ cm}^{-1}$ are strong in chlorites [92].

723

724 **Raw clay examples**

725 Example FTIR spectra of raw clays evaluated for use as SCM are shown in Figure 8. For kaolinitic clays
726 (K1 and K2), the characteristic band at 3700 cm^{-1} is isolated from absorption bands of most other clay
727 minerals allowing the identification of very low kaolinite concentrations [85]. The four characteristic
728 bands (3690 , 3670 , 3650 and 3620 cm^{-1}) are well defined in K1 indicating that K1 contains ordered
729 kaolinite, in K2 the intermediate bands (3670 and 3650) are absent indicating disordered kaolinite
730 [95]. For halloysite clay (H) [96], the bands at 3700 and 3620 cm^{-1} in Figure 8 are assigned to internal
731 surface OH groups. The weak band at 3570 cm^{-1} present in halloysite may arise from H-bonding
732 between surface OH- groups and interlayer water [92].

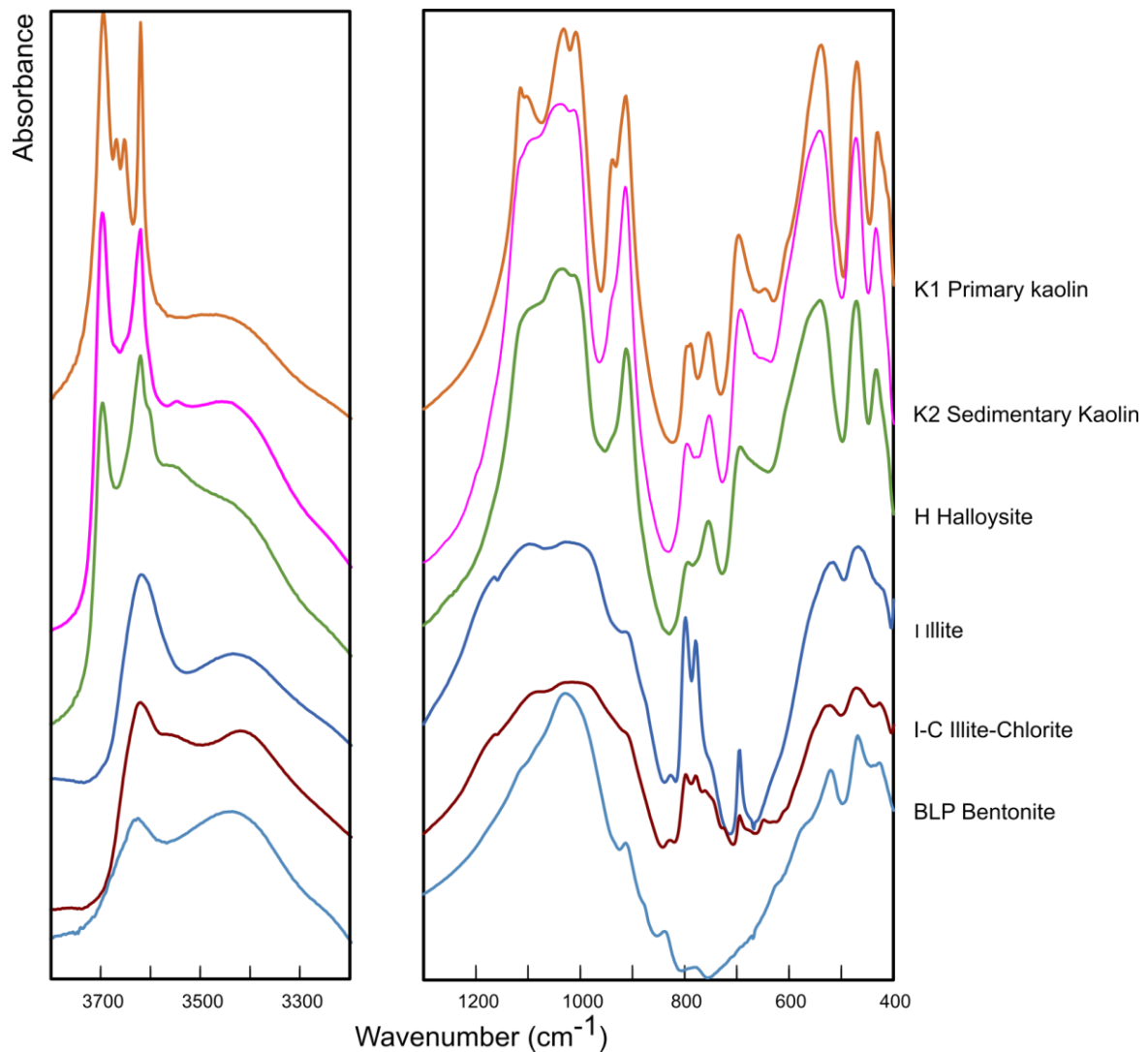
733

734 For illitic shale [97], the FTIR spectrum (Figure 8) shows the OH- stretching band at 3624 cm^{-1}
735 accompanied by a strong absorption at 3423 cm^{-1} that is allocated to OH stretching vibrations of water
736 molecules not released upon heating of the KBr pellet [94]. The Si-O stretching band is present at 1027
737 cm^{-1} , and a doublet in the $825\text{--}750\text{ cm}^{-1}$ range is assigned to the vibration of Si-O-Al moieties [98].
738 Figure 8 also includes a raw clay (illite -chlorite, I-C) showing a weak inflection at 3680 cm^{-1} and strong
739 bands of OH bending [16]. Bentonite [99] contains montmorillonite showing a OH stretching band at
740 3623 cm^{-1} [90] and the vibration bands of the different groups of montmorillonites are also present.

741

742 Whilst MIR spectroscopy does not offer the same opportunities for quantitative mineralogical analysis
743 as in XRD and STA, its speed and relative simplicity nonetheless offers advantages – particularly for
744 broadly identifying the presence of 1:1 and/or 2:1 clay minerals, based on the number and profile of
745 OH-stretching absorption bands in the $3500\text{--}3800\text{ cm}^{-1}$ range, and complementary information about
746 structural ordering.

747



748

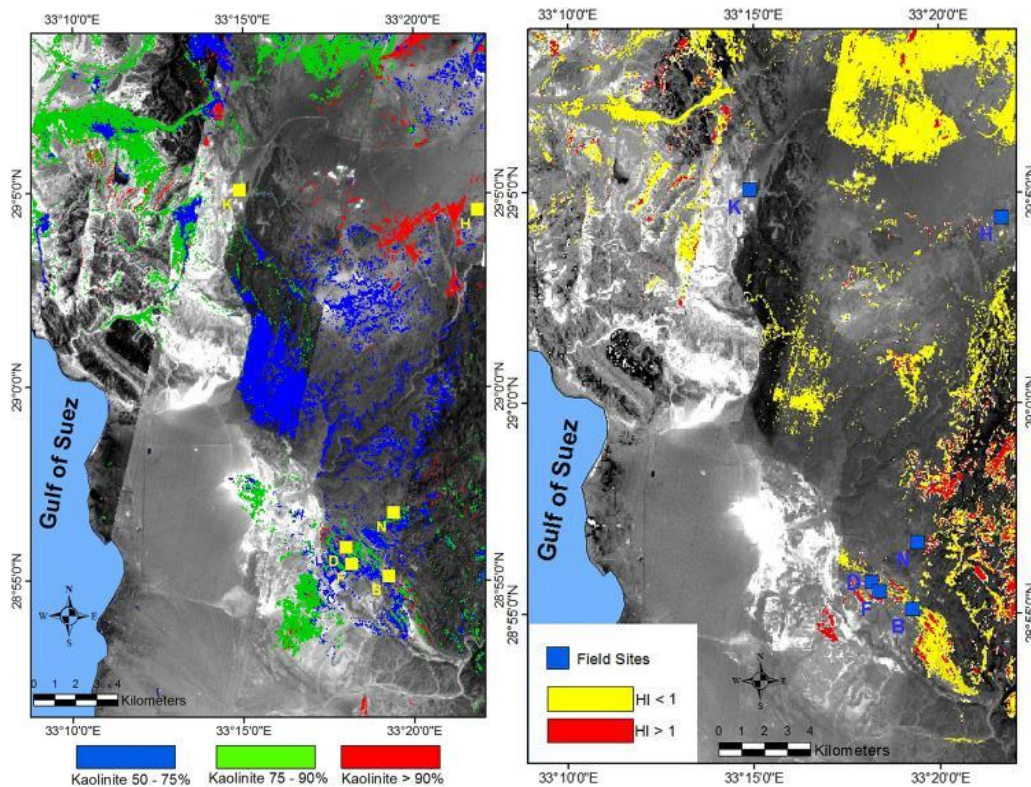
749 *Figure 8. IR Spectra of raw clays evaluated for use as SCM: a) and b) kaolinitic clay [95], c) halloysite*
 750 *[96]; d) illitic shale [97]; e) Illitic-chlorite shale [16], and f) bentonite [100].*

751

3.4.2. Remote sensing for clay prospecting

752 Whilst laboratory-based infrared spectroscopy typically focusses on the near- and mid-infrared
 753 spectral range (13000-1250 cm⁻¹), the visible and near infrared (VNIR) range (25000-9000 cm⁻¹) offers
 754 specific opportunities for remote sensing.

755 The principle of spectroscopy-based remote sensing is that airborne or satellite-mounted sensors
 756 measure the reflectance radiation from the earth's surface for either a small number of wavelength
 757 channels (multi-spectral) or a continuum of wavelengths (hyper-spectral). The mineralogy (along with
 758 other aspects) of the area can be identified by comparing the measured signals to spectral libraries,
 759 and then mapped [101]. Previous studies have used VNIR remote sensing to: map the distribution of
 760 different clay minerals in soils [102, 103]; estimate the overall clay content of soils [104], and (in
 761 combination with XRD analysis to facilitate supervised classification) map kaolinite deposits by both
 762 purity (%kaolinite) and quality (degree of disorder) (Figure 9) [105].



763

764 *Figure 9. Hyperspectral maps showing the distribution of a) kaolin purity and b) kaolinite Hinckley Index*
 765 *for a kaolin deposit in Egypt. Images reprinted with permission from [105].*

766 The key advantage of remote sensing is the potential to produce mineralogical maps of large areas
 767 very quickly, with drone-based systems offering an additional advantage of low cost [106]. The main
 768 drawbacks and limitations are around measurement (sampling depth, spatial resolution and
 769 vegetation cover), as well as the spectral resolution and sensitivity of the instruments themselves. It
 770 is also advised not to solely rely on remote measurements, but to support with validation from some
 771 terrestrial measurements [107]. More detailed information on the capabilities and limitations of the
 772 different instruments and systems available can be found elsewhere [108, 109].

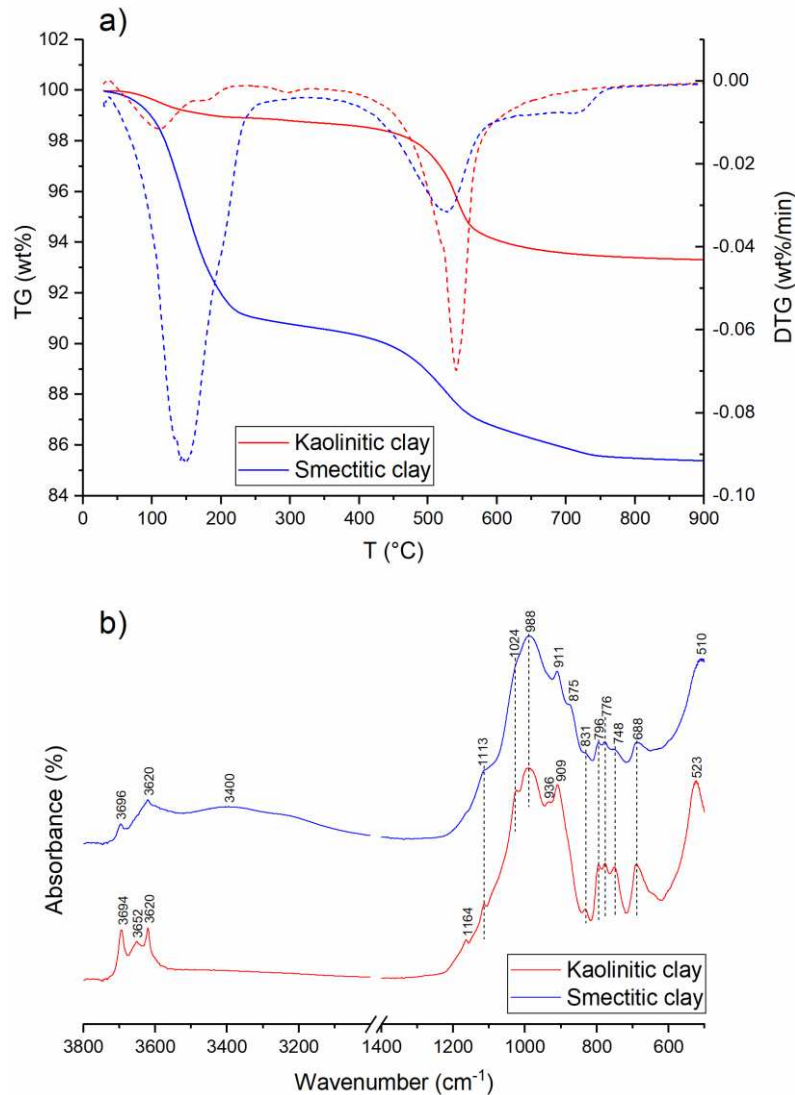
773 VNIR remote sensing has shown great progress in mapping of soils in recent years (e.g. Global Soils
 774 Map project) [110], but has yet to be exploited much for clays prospecting in the cement industry.
 775 These techniques could be adapted to play a key role in the triage of analysing deposits in remote
 776 and/or poorly documented areas, supporting exploitation of a wider variety of deposits for localised
 777 production, especially in developing countries.

778 **4. Case studies**

779 Two exemplary case studies are discussed here to illustrate the mineralogical interpretation and
 780 analysis two impure clays, i.e. one quartz-rich kaolinitic clay and one smectitic clay, both originating
 781 from the German Westerwald area. Both clays were measured by XRD, TGA and FTIR spectroscopy,
 782 the samples were prepared in line with the general guidelines provided in the respective sections.

783
 784 The XRD measurements are plotted in Figure 10, measurements were made of a randomly oriented
 785 bulk sample of each clay, and of oriented specimens of the clay size fraction (< 2 μm). Air-dried,
 786 ethylene glycol (EG) solvated and 550 °C heat treated oriented specimens were prepared and
 787 measured to support the mineralogical interpretation. The XRD results show that the kaolinitic clay is
 788 mainly composed of the clay minerals kaolinite and illite, together with quartz and traces of other
 789 minerals such as feldspars. The identification of kaolinite is confirmed by the absence of its (001) peaks
 790 in the heat treated oriented specimen. The presence of chlorite can be excluded due to the absence

824 clays, the latter only in the kaolinitic clay. The additional vibration band at 875 cm⁻¹ in the smectitic
 825 clay indicates substitution of Al by Fe³⁺ in the montmorillonite (smectite) octahedral sheet.
 826



827
 828 *Figure 11. TG/DTG (a) and FTIR (b) measurements of the case study impure kaolinitic and smectitic*
 829 *clays. In (a) the TG curves are displayed as solid lines and the DTG curves as dashed lines. In (b) the*
 830 *wavenumbers of the vibration bands are indicated.*

831 Quantitative phase analysis of the bulk samples was made by Rietveld refinement using the software
 832 Profex-BGMN [58]. The program allows an implementation of disorder models, e.g. turbostratic
 833 disorder in smectites or stacking disorder in kaolinite. In order to retrieve absolute phase contents
 834 and the amount of amorphous or unknown phases, the scale factors were normalized to an external
 835 standard [46]. Therefore, the mass attenuation coefficient of each sample was calculated, based on
 836 the chemical composition.

837 *Table 2. Quantitative phase analysis results of the case study kaolinitic and smectitic clays as obtained*
 838 *by XRD-Rietveld refinement*

Phase	Kaolinitic clay (mass%)	Smectitic clay (mass%)
Kaolinite	27.3	8.4
Illite/Muscovite	25.4	3.6
Montmorillonite	-	62.5
Quartz	41.0	14.2

Feldspar	2.3	4.7
Calcite	-	1.3
Rutile/Anatase	1.4	1.4
Iron oxides/hydroxides	1.5	
Amorphous/unknown phase	1.1	3.8

839

840 The quantitative phase analysis is in good agreement with the TGA results. Regarding the kaolinitic
841 clay, a mass loss of 5.4 wt% occurs between 400 and 1000 °C. The dehydroxylation of kaolinite
842 accounts for 3.8 wt%, based on its chemical formula and the mass content derived by XRD. This would
843 leave 1.6 wt% mass loss attributed to illite/muscovite.

844

845 Further to the information provided in this article, the interested reader is recommended to seek out
846 the Baseline Studies of the Clay Minerals Society Source Clays³ [111]. Whilst many advances in terms
847 of techniques have been made since their publication in the early 2000s, they remain a highly useful
848 (and free to access) collection of detailed characterization studies using the techniques described
849 here, carried out on the clay minerals of primary interest to cement scientists.

850 5. Summary and perspectives

851 The rapid development of calcined clay blended cements requires accessible and robust techniques
852 to characterise the mineralogical composition of potentially suitable clay resources. Before setting out
853 on clay analysis techniques, this paper stresses the importance of field sampling methodology and
854 sample preparation to obtain representative specimens. If not done properly, any subsequent
855 analysis, no matter how meticulously carried out, risks to be biased and of little use.

856

857 Three characterisation techniques were identified to be most relevant, XRD, thermal analysis and IR
858 spectroscopy. They have in common that they are easily accessible and well-established in most
859 cement chemistry laboratories, and have been extensively applied to clay science. Due to the fine-
860 grained and multi-phase nature of clays, and the structural and compositional variability of the clay
861 minerals, mineralogical analysis of clays is often tedious, and practitioners should be aware of
862 potential interferences and limitations. Therefore, for each of the techniques, clay specific sample
863 preparation and data collection routines were described together with guidelines to the interpretation
864 and analysis of the collected data.

865 XRD is of great practical value in clay mineralogy. Even for highly complex clays and clay minerals, it
866 can provide both highly resolved identification of clay and other minerals and accurate phase
867 quantification. To obtain such information, specific laboratory routines and analytical software are
868 required, using these correctly relies on somewhat advanced understanding and analytical
869 experience.

870 Thermal analysis can be used more readily and easily, yet does not provide the same level of detail as
871 XRD. Overlap between mass loss events for different clay minerals can be significant. Similarly,
872 structural and chemical variability of individual clay minerals affect the heating profiles considerably.
873 Both phenomena interfere with accurate phase quantification. A notable exception may be kaolinite-
874 group minerals, that show a rather distinct and pronounced dehydroxylation event, enabling a fairly
875 accurate estimation of their total content by thermal analysis.

876 IR spectroscopy is straightforward to use, but should mainly be seen as a complementary qualitative
877 technique that provides information on structural (dis)order or averaged octahedral layer composition
878 that is more difficult to obtain using XRD and thermal analysis. IR spectroscopy can also be used as
879 identification technique for exploration purposes, such as remote sensing, or made portable for in-
880 situ field measurements. Interpretation is more difficult for complex multi-phase clays.

881

³ available at [Baseline/MSDS studies of source clays – The Clay Minerals Society](#)

882 As clay purity and the type and content of accompanying minerals are important characteristics that
883 define the suitability as SCM resource, mineralogical characterisation is indispensable as source of
884 information. Moreover, to better understand and predict the performance of the broad and
885 heterogeneous group of 2:1 clays, much more detailed research based on a solid and extensive
886 analysis of the clay mineralogy is needed.

887
888

889 **Declarations and statements**

890 The contents of this paper reflect the views of the authors, who are responsible for the validity and
891 accuracy of presented data, and do not necessarily reflect the views of their affiliated organisations.

892
893

893 **Author contributions**

894 Initiation and conceptualisation: Ruben Snellings and Adrian Alujas Diaz; Data provision and
895 processing: Matthias Maier, Ruben Snellings and Edgardo F. Irassar; Writing of sections: Ruben
896 Snellings, Adrian Alujas Diaz, Theodore Hanein, Edgardo F. Irassar, Matthias Maier, Alastair T. Marsh,
897 Luca Valentini, Franco Zunino; Critical revising: Fragkoulis Kanavaris, Roger Almenares, Theodore
898 Hanein, Matthias Maier, Alastair T. Marsh, Adrian Alujas Diaz; Coordination, integration and editing:
899 Ruben Snellings and Adrian Alujas Diaz.

900
901

901 **Funding**

902 Participation of Alastair T. Marsh was funded by EPSRC EP/R001642/1. Participation of T. Hanein was
903 funded by UKRI through the Circular Economy Centre for Mineral-based Construction Materials
904 (EP/V011820/1). The other authors received no support from any organization for the submitted
905 work.

906
907

907 **Competing interests**

908 The authors have no competing interests to declare that are relevant to the content of this article.

909
910

910 **Acknowledgements**

911 Textual comments and suggestions by Alisa Machner are gratefully acknowledged.

912
913

913 **References**

- 914 1. Juenger, M.C., R. Snellings, and S.A. Bernal, *Supplementary cementitious materials:*
915 *New sources, characterization, and performance insights*. Cement and Concrete
916 Research, 2019. **122**: p. 257-273.
- 917 2. Scrivener, K., et al., *Calcined clay limestone cements (LC3)*. Cement and Concrete
918 Research, 2018. **114**: p. 49-56.
- 919 3. Scrivener, K.L., V.M. John, and E.M. Gartner, *Eco-efficient cements: potential,*
920 *economically viable solutions for a low-CO₂, cement-based materials industry*, in *UNEP*
921 *Report*. 2016, United Nations Environment Programme: Paris. p. 50.
- 922 4. Maier, M., N. Beuntner, and K.-C. Thienel, *Mineralogical characterization and*
923 *reactivity test of common clays suitable as supplementary cementitious material*.
924 Applied Clay Science, 2021. **202**: p. 105990.
- 925 5. Hollanders, S., et al., *Pozzolanic reactivity of pure calcined clays*. Applied Clay Science,
926 2016. **132**: p. 552-560.
- 927 6. Skibsted, J. and R. Snellings, *Reactivity of supplementary cementitious materials*
928 *(SCMs) in cement blends*. Cement and Concrete Research, 2019. **124**: p. 105799.
- 929 7. Brindley, G. and G. Brown, *Quantitative X-ray mineral analysis of clays*. Crystal
930 structures of clay minerals and their X-ray identification, 1980. **5**: p. 411-438.

- 931 8. Moore, D.M. and R.C.J. Reynolds, *X-ray Diffraction and the Identification and Analysis*
932 *of Clay Minerals*. 2nd ed. 1997, Oxford, New York: Oxford University Press (OUP).
- 933 9. Raven, M.D. and P.G. Self, *Outcomes of 12 years of the Reynolds Cup quantitative*
934 *mineral analysis round robin*. *Clays and Clay Minerals*, 2017. **65**(2): p. 122-134.
- 935 10. Omotoso, O., et al., *Some successful approaches to quantitative mineral analysis as*
936 *revealed by the 3rd Reynolds Cup contest*. *Clays and Clay Minerals*, 2006. **54**(6): p. 748-
937 760.
- 938 11. Środoń, J., *Identification and quantitative analysis of clay minerals*. *Developments in*
939 *Clay Science*, 2006. **1**: p. 765-787.
- 940 12. Avet, F. and K. Scrivener, *Investigation of the calcined kaolinite content on the*
941 *hydration of Limestone Calcined Clay Cement (LC3)*. *Cement and Concrete Research*,
942 2018. **107**: p. 124-135.
- 943 13. Alujas, A., et al., *Pozzolanitic reactivity of low grade kaolinitic clays: Influence of*
944 *calcination temperature and impact of calcination products on OPC hydration*. *Applied*
945 *Clay Science*, 2015. **108**: p. 94-101.
- 946 14. Snellings, R., et al., *Properties and pozzolanitic reactivity of flash calcined dredging*
947 *sediments*. *Applied Clay Science*, 2016. **129**: p. 35-39.
- 948 15. Danner, T., G. Norden, and H. Justnes, *Characterisation of calcined raw clays suitable*
949 *as supplementary cementitious materials*. *Applied Clay Science*, 2018. **162**: p. 391-402.
- 950 16. Irassar, E.F., et al., *Calcined illite-chlorite shale as supplementary cementing material:*
951 *Thermal treatment, grinding, color and pozzolanitic activity*. *Applied Clay Science*, 2019.
952 **179**: p. 105143.
- 953 17. Konta, J. and R. Kühnel, *Integrated exploration of clay deposits: Some changes of*
954 *strategy*. *Applied clay science*, 1997. **11**(5-6): p. 273-283.
- 955 18. Andresen, A., *Exploration, sampling and in-situ testing of soft clay*. 1981.
- 956 19. Potts, P.J. and P. Robinson, *Sample preparation of geological samples, soils and*
957 *sediments*. 2003.
- 958 20. Potts, P.J. and M. West, *Portable X-ray fluorescence spectrometry: Capabilities for in*
959 *situ analysis*. 2008: Royal Society of Chemistry.
- 960 21. Rousseau, R., *Concept of the influence coefficient*. *Rigaku J*, 2001. **18**(1): p. 8-14.
- 961 22. Ichikawa, S. and T. Nakamura, *Approaches to solid sample preparation based on*
962 *analytical depth for reliable X-ray fluorescence analysis*. *X-Ray Spectrometry*, 2016.
963 **45**(6): p. 302-307.
- 964 23. Hou, X., Y. He, and B.T. Jones, *Recent advances in portable X-ray fluorescence*
965 *spectrometry*. *Applied Spectroscopy Reviews*, 2004. **39**(1): p. 1-25.
- 966 24. Weindorf, D.C., N. Bakr, and Y. Zhu, *Advances in portable X-ray fluorescence (PXRF) for*
967 *environmental, pedological, and agronomic applications*. *Advances in agronomy*,
968 2014. **128**: p. 1-45.
- 969 25. Horta, A., et al., *Potential of integrated field spectroscopy and spatial analysis for*
970 *enhanced assessment of soil contamination: a prospective review*. *Geoderma*, 2015.
971 **241**: p. 180-209.
- 972 26. Liangquan, G., *Geochemical prospecting*, in *Portable X-ray Fluorescence Spectrometry*.
973 2008, Royal Society of Chemistry: Cambridge, UK. p. 141-173.
- 974 27. Stockmann, U., et al., *Utilizing portable X-ray fluorescence spectrometry for in-field*
975 *investigation of pedogenesis*. *Catena*, 2016. **139**: p. 220-231.

- 976 28. Silva, S.H.G., et al., *Soil weathering analysis using a portable X-ray fluorescence (PXRF)*
977 *spectrometer in an Inceptisol from the Brazilian Cerrado*. Applied Clay Science, 2018.
978 **162**: p. 27-37.
- 979 29. Olesik, J.W., *Peer reviewed: Fundamental research in ICP-OES and ICPMS*. Analytical
980 Chemistry, 1996. **68**(15): p. 469A-474A.
- 981 30. Carter, J.A., et al., *Traditional calibration methods in atomic spectrometry and new*
982 *calibration strategies for inductively coupled plasma mass spectrometry*. Frontiers in
983 chemistry, 2018. **6**: p. 504.
- 984 31. Batista, A.H., R.J. Gilkes, and A.W. Rate, *Relationship between heavy metals and*
985 *minerals extracted from soil clay by standard and novel acid extraction procedures*.
986 Environmental monitoring and assessment, 2016. **188**(12): p. 1-18.
- 987 32. Janotková, I., et al., *Comparison of inductively coupled plasma optical emission*
988 *spectrometry, energy dispersive X-ray fluorescence spectrometry and laser ablation*
989 *inductively coupled plasma mass spectrometry in the elemental analysis of agricultural*
990 *soils*. Journal of Analytical Atomic Spectrometry, 2013. **28**(12): p. 1940-1948.
- 991 33. Khalifa, A.Z., et al., *Comparing the reactivity of different natural clays under thermal*
992 *and alkali activation*. RILEM Technical Letters, 2019. **4**: p. 74-80.
- 993 34. Bergaya, F., B.K.G. Theng, and G. Lagaly, *Chapter 12 Critical Assessment of Some*
994 *Analytical Techniques*. 2006. **1**: p. 753-754.
- 995 35. Jackson, M.L., *Soil chemical analysis: Advanced course*. 2005: UW-Madison Libraries
996 Parallel Press.
- 997 36. Poppe, L., et al., *A laboratory manual for X-ray powder diffraction*. US Geological
998 Survey open-file report, 2001. **1**(041): p. 1-88.
- 999 37. Środoń, J., *Chapter 2.2-Identification and Quantitative Analysis of Clay Minerals*. F. B.
1000 and G. Lagaly (Ed.), *Developments in Clay Science*, 2013. **5**: p. 25-49.
- 1001 38. Kleeberg, R., T. Monecke, and S. Hillier, *Preferred orientation of mineral grains in*
1002 *sample mounts for quantitative XRD measurements: How random are powder*
1003 *samples?* Clays and clay minerals, 2008. **56**(4): p. 404-415.
- 1004 39. Bish, D.L. and R. Reynolds, *4. SAMPLE PREPARATION FOR X-RAY DIFFRACTION*. Modern
1005 powder diffraction, 2018: p. 73-100.
- 1006 40. Steudel, A. and K. Emmerich, *Strategies for the successful preparation of homoionic*
1007 *smectites*. Applied Clay Science, 2013. **75**: p. 13-21.
- 1008 41. Méring, J., *L'interférence des rayons X dans les systèmes à stratification désordonnée*.
1009 Acta Crystallographica, 1949. **2**(6): p. 371-377.
- 1010 42. Ufer, K., R. Kleeberg, and T. Monecke, *Quantification of stacking disordered Si-Al layer*
1011 *silicates by the Rietveld method: application to exploration for high-sulphidation*
1012 *epithermal gold deposits*. Powder Diffraction, 2015. **30**(S1): p. S111.
- 1013 43. Madsen, I., et al., *Quantitative phase analysis*. 2019.
- 1014 44. Zhou, X., et al., *XRD-based quantitative analysis of clay minerals using reference*
1015 *intensity ratios, mineral intensity factors, Rietveld, and full pattern summation*
1016 *methods: A critical review*. Solid Earth Sciences, 2018. **3**(1): p. 16-29.
- 1017 45. Hillier, S., *Accurate quantitative analysis of clay and other minerals in sandstones by*
1018 *XRD: comparison of a Rietveld and a reference intensity ratio (RIR) method and the*
1019 *importance of sample preparation*. Clay minerals, 2000. **35**(1): p. 291-302.
- 1020 46. O'Connor, B.H. and M.D. Raven, *Application of the Rietveld Refinement Procedure in*
1021 *Assaying Powdered Mixtures*. Powder Diffraction, 1988. **3**(1): p. 2-6.

- 1022 47. Środoń, J., *Chapter 12.2 Identification and Quantitative Analysis of Clay Minerals*.
1023 2006. **1**: p. 765-787.
- 1024 48. Bish, D.L. and S. Howard, *Quantitative phase analysis using the Rietveld method*.
1025 *Journal of Applied Crystallography*, 1988. **21**(2): p. 86-91.
- 1026 49. Butler, B.M. and S. Hillier, *Automated full-pattern summation of X-ray powder*
1027 *diffraction data for high-throughput quantification of clay-bearing mixtures*. *Clays and*
1028 *Clay Minerals*, 2021: p. 1-14.
- 1029 50. Chipera, S.J. and D.L. Bish, *FULLPAT: a full-pattern quantitative analysis program for*
1030 *X-ray powder diffraction using measured and calculated patterns*. *Journal of Applied*
1031 *Crystallography*, 2002. **35**(6): p. 744-749.
- 1032 51. Mystkowski, K., J. Srodon, and D. McCarty. *Application of evolutionary programming*
1033 *to automatic XRD quantitative analysis of clay-bearing rocks*. in *The Clay Minerals*
1034 *Society 39th Annual Meeting, Boulder, Colorado, Abstracts with Programs*. 2002.
- 1035 52. Eberl, D., *User guide to RockJock-A program for determining quantitative mineralogy*
1036 *from X-ray diffraction data*. 2003, US Geological Survey.
- 1037 53. Butler, B. and S. Hillier, *powdR: Full Pattern Summation of X-Ray Powder Diffraction*
1038 *Data, in R package version*. 2020.
- 1039 54. Butler, B.M. and S. Hillier, *powdR: An R package for quantitative mineralogy using full*
1040 *pattern summation of X-ray powder diffraction data*. *Computers & Geosciences*, 2021.
1041 **147**: p. 104662.
- 1042 55. Rietveld, H.M., *A profile refinement method for nuclear and magnetic structures*.
1043 *Journal of applied Crystallography*, 1969. **2**(2): p. 65-71.
- 1044 56. Ufer, K. and M.D. Raven, *Application of the Rietveld method in the Reynolds cup*
1045 *contest*. *Clays and Clay Minerals*, 2017. **65**(4): p. 286-297.
- 1046 57. Bergmann, J. and R. Kleeberg. *Rietveld analysis of disordered layer silicates*. in
1047 *Materials Science Forum*. 1998. Trans Tech Publ.
- 1048 58. Doebelin, N. and R. Kleeberg, *Profex: a graphical user interface for the Rietveld*
1049 *refinement program BGMN*. *Journal of Applied Crystallography*, 2015. **48**(5): p. 1573-
1050 1580.
- 1051 59. Coelho, A.A., J.S. Evans, and J.W. Lewis, *Averaging the intensity of many-layered*
1052 *structures for accurate stacking-fault analysis using Rietveld refinement*. *Journal of*
1053 *Applied Crystallography*, 2016. **49**(5): p. 1740-1749.
- 1054 60. Coelho, A.A., *TOPAS and TOPAS-Academic: an optimization program integrating*
1055 *computer algebra and crystallographic objects written in C++*. *Journal of Applied*
1056 *Crystallography*, 2018. **51**(1): p. 210-218.
- 1057 61. Scarlett, N.V.Y. and I.C. Madsen, *Quantification of phases with partial or no known*
1058 *crystal structures*. *Powder Diffraction*, 2006. **21**(04): p. 278-284.
- 1059 62. Aranda, M.A., A.G. De la Torre, and L. León-Reina, *Rietveld quantitative phase analysis*
1060 *of OPC clinkers, cements and hydration products*. *Reviews in Mineralogy and*
1061 *Geochemistry*, 2012. **74**(1): p. 169-209.
- 1062 63. Todor, D.N., *Thermal analysis of minerals*. 1976: Abacus press.
- 1063 64. Karathanasis, A. and W. Harris, *Quantitative thermal analysis of soil materials*.
1064 *Quantitative methods in soil mineralogy*, 1994: p. 360-411.
- 1065 65. Le Chatelier, H., *De l'action de la chaleur sur les argiles*. *Bulletin de Minéralogie*, 1887.
1066 **10**(5): p. 204-211.
- 1067 66. Giese, R., *Differential scanning calorimetry of clay minerals and their intercalates*.
1068 *Thermal analysis in clay science*. Clay Minerals Society, 1990: p. 10-48.

- 1069 67. Rouquerol, F., J. Rouquerol, and P. Llewellyn, *Thermal Analysis*, in *Thermal analysis in*
1070 *Clay Science*, F. Bergaya and G. Lagaly, Editors. 2013, Elsevier. p. 361-379.
- 1071 68. Földvári, M., *Handbook of thermogravimetric system of minerals and its use in*
1072 *geological practice*. Vol. 213. 2011: Geological Institute of Hungary Budapest.
- 1073 69. Bish, D.L., C.J. Duffy, and R.F. Giese, *Thermal Analysis in Clay Science*. CMS workshop
1074 lectures. Vol. 3. 1990, Boulder: The Clay Minerals Society. 192.
- 1075 70. Karathanasis, A. and B. Hajek, *Revised methods for rapid quantitative determination*
1076 *of minerals in soil clays*. Soil Science Society of America Journal, 1982. **46**(2): p. 419-
1077 425.
- 1078 71. Vaculikova, L., et al., *Characterization and differentiation of kaolinites from selected*
1079 *Czech deposits using infrared spectroscopy and differential thermal analysis*. 2011.
- 1080 72. Smykatz-Kloss, W., *The determination of the degree of (dis-) order of kaolinites by*
1081 *means of differential thermal analysis*. Chemie der Erde, 1974. **33**: p. 358-364.
- 1082 73. Ptáček, P., et al., *The influence of structure order on the kinetics of dehydroxylation of*
1083 *kaolinite*. Journal of the European Ceramic Society, 2013. **33**(13-14): p. 2793-2799.
- 1084 74. Lorentz, B., et al., *Characterization of Florida kaolin clays using multiple-technique*
1085 *approach*. Applied Clay Science, 2018. **161**: p. 326-333.
- 1086 75. Plante, A.F., J.M. Fernández, and J. Leifeld, *Application of thermal analysis techniques*
1087 *in soil science*. Geoderma, 2009. **153**(1-2): p. 1-10.
- 1088 76. Fernandez, R., F. Martirena, and K.L. Scrivener, *The origin of the pozzolanic activity of*
1089 *calcined clay minerals: A comparison between kaolinite, illite and montmorillonite*.
1090 Cement and Concrete Research, 2011. **41**(1): p. 113-122.
- 1091 77. Marsh, A., et al., *Influence of clay minerals and associated minerals in alkali activation*
1092 *of soils*. Construction and Building Materials, 2019. **229**: p. 116816.
- 1093 78. Mackenzie, R. and S. Caillere, *The thermal characteristics of soil minerals and the use*
1094 *of these characteristics in the qualitative and quantitative determination of clay*
1095 *minerals in soils*, in *Soil components*. 1975, Springer. p. 529-571.
- 1096 79. Hayakawa, T., et al., *Modified method for bentonite purification and characterization;*
1097 *A case study using bentonite from Tsunagi Mine, Niigata, Japan*. Clays and Clay
1098 Minerals, 2016. **64**(3): p. 275-282.
- 1099 80. Alujas, A., et al., *Pozzolanic reactivity of low grade kaolinitic clays: influence of*
1100 *mineralogical composition*, in *Calcined Clays for Sustainable Concrete*. 2015, Springer.
1101 p. 339-345.
- 1102 81. Avet, F. and K. Scrivener, *Simple and reliable quantification of kaolinite in clay using*
1103 *an oven and a balance*. Calcined Clays for Sustainable Concrete, RILEM Bookseries;
1104 Springer: Dordrecht, The Netherlands, 2020. **15**: p. 147-156.
- 1105 82. Bernal, S.A., et al., *Characterization of supplementary cementitious materials by*
1106 *thermal analysis*. Materials and Structures, 2017. **50**(1): p. 1-13.
- 1107 83. Chryssikos, G., *Modern Infrared and Raman Instrumentation and Sampling Methods*,
1108 in *Developments in Clay Science*. 2017, Elsevier. p. 34-63.
- 1109 84. Gates, W., et al., *Infrared and Raman spectroscopies of clay minerals*. 2017: Elsevier.
- 1110 85. Madejova, J. and P. Komadel, *Baseline studies of the clay minerals society source clays:*
1111 *infrared methods*. Clays and clay minerals, 2001. **49**(5): p. 410-432.
- 1112 86. Madejová, J., W. Gates, and S. Petit, *IR spectra of clay minerals*, in *Developments in*
1113 *clay science*. 2017, Elsevier. p. 107-149.
- 1114 87. Hutengs, C., et al., *Comparison of portable and bench-top spectrometers for mid-*
1115 *infrared diffuse reflectance measurements of soils*. Sensors, 2018. **18**(4): p. 993.

- 1116 88. Balan, E., et al., *First-principles modeling of the infrared spectrum of kaolinite*. American Mineralogist, 2001. **86**(11-12): p. 1321-1330.
- 1117
- 1118 89. Balan, E., et al., *First-principles study of OH-stretching modes in kaolinite, dickite, and*
1119 *nacrite*. American Mineralogist, 2005. **90**(1): p. 50-60.
- 1120 90. Madejová, J., *FTIR techniques in clay mineral studies*. Vibrational Spectroscopy, 2003.
1121 **31**(1): p. 1-10.
- 1122 91. Bich, C., J. Ambroise, and J. Péra, *Influence of degree of dehydroxylation on the*
1123 *pozzolanic activity of metakaolin*. Applied Clay Science, 2009. **44**(3-4): p. 194-200.
- 1124 92. Russell, J. and A. Fraser, *Infrared methods*, in *Clay Mineralogy: Spectroscopic and*
1125 *chemical determinative methods*. 1994, Springer. p. 11-67.
- 1126 93. Hillier, S., et al., *Correlations among the mineralogical and physical properties of*
1127 *halloysite nanotubes (HNTs)*. Clay Minerals, 2016. **51**(3): p. 325-350.
- 1128 94. Farmer, V.C., *Infrared spectra of minerals*. 1974: Mineralogical society.
- 1129 95. Tironi, A., et al., *Potential use of Argentine kaolinitic clays as pozzolanic material*.
1130 Applied Clay Science, 2014. **101**: p. 468-476.
- 1131 96. Tironi, A., et al., *Pozzolanic activity of calcined halloysite-rich kaolinitic clays*. Applied
1132 Clay Science, 2017. **147**: p. 11-18.
- 1133 97. Irassar, E.F., et al., *Thermal Treatment and Pozzolanic Activity of Calcined Clay and*
1134 *Shale*. ACI Materials Journal, 2019. **116**(4).
- 1135 98. Vaculikova, L. and E. Plevova, *Identification of clay minerals and micas in sedimentary*
1136 *rocks*. Acta Geodynamica et geomaterialia, 2005. **2**(2): p. 163.
- 1137 99. Tironi, A., et al., *Kaolinitic calcined clays: Factors affecting its performance as*
1138 *pozzolans*. Construction and Building Materials, 2012. **28**(1): p. 276-281.
- 1139 100. Tironi, A., et al., *Thermal activation of bentonites for their use as pozzolan*. Revista de
1140 la Construccion, 2012. **11**(1): p. 44-53.
- 1141 101. Mulder, V., et al., *The use of remote sensing in soil and terrain mapping—A review*.
1142 Geoderma, 2011. **162**(1-2): p. 1-19.
- 1143 102. Chabrilat, S., et al., *Use of hyperspectral images in the identification and mapping of*
1144 *expansive clay soils and the role of spatial resolution*. Remote sensing of Environment,
1145 2002. **82**(2-3): p. 431-445.
- 1146 103. Mulder, V., et al., *Characterizing regional soil mineral composition using spectroscopy*
1147 *and geostatistics*. Remote sensing of environment, 2013. **139**: p. 415-429.
- 1148 104. Gasmi, A., et al., *Surface soil clay content mapping at large scales using multispectral*
1149 *(VNIR–SWIR) ASTER data*. International Journal of Remote Sensing, 2019. **40**(4): p.
1150 1506-1533.
- 1151 105. Awad, M.E., et al., *Hyperspectral remote sensing for mapping and detection of*
1152 *Egyptian kaolin quality*. Applied Clay Science, 2018. **160**: p. 249-262.
- 1153 106. Zhong, Y., et al., *Mini-UAV-borne hyperspectral remote sensing: From observation and*
1154 *processing to applications*. IEEE Geoscience and Remote Sensing Magazine, 2018. **6**(4):
1155 p. 46-62.
- 1156 107. Kirsch, M., et al., *Integration of terrestrial and drone-borne hyperspectral and*
1157 *photogrammetric sensing methods for exploration mapping and mining monitoring*.
1158 Remote Sensing, 2018. **10**(9): p. 1366.
- 1159 108. Fang, Q., et al., *Visible and near-infrared reflectance spectroscopy for investigating soil*
1160 *mineralogy: A review*. Journal of Spectroscopy, 2018. **2018**.

- 1161 109. Van der Meer, F.D., et al., *Multi-and hyperspectral geologic remote sensing: A review.*
1162 International Journal of Applied Earth Observation and Geoinformation, 2012. **14**(1):
1163 p. 112-128.
- 1164 110. Arrouays, D., et al., *McBratney AB, McKenzie NJ, Mendonca-Santos MdL, Minasny B,*
1165 *Montanarella L., Odeh IOA, Sanchez PA, Thompson JA et Zhang G.-L., 2014-*
1166 *GlobalSoilMap: Toward a Fine-Resolution Global Grid of Soil Properties.* Advances in
1167 Agronomy. **125**: p. 93-134.
- 1168 111. Costanzo, P.M., *Baseline studies of the clay minerals society source clays: Introduction.*
1169 Clays and Clay Minerals, 2001. **49**(5): p. 372-373.
- 1170 112. Thorez, J., *Phyllosilicates and Clay minerals: a Laboratory Handbook for their X-ray*
1171 *Diffraction Analysis.* 1975.
- 1172 113. Chukanov, N.V., *Infrared spectra of mineral species: extended library.* 2013: Springer
1173 Science & Business Media.

1174

1175

1176 **Annex I. XRD search table for clay minerals and commonly associated phases**

1177

1178 *Table 3. Search Table (modified after Brindley and Brown (1980) [7] and Thorez (1975) [112])*

d	Clay minerals and phyllosilicates	d	Other silicates	d	Oxides, hydroxides, carbonates, sulfate, etc.
17-0-16-8	Smectite, glycol (10)				
15-5-15	Smectite, Mg Ca (10)				
14-6-14	Vermiculite (10)				
14-3-14-0	Chlorite (3-10), weak if iron-rich				
14-1-13-7	Chlorite, 500-600°C (10+)				
12-4	Smectite, Na (10)				
12-3-12-0	Sepiolite (10)				
10-5-10-3	Palygorskite (10)				
10-1-10-0	Halloysite – 10 Å (7-10)				
10-1-9-9	Muscovite (10) Phlogopite (10)				
	Biotite (10)				
10-9-6	Smectite, collapsed (10)				
	Vermiculite, collapsed (10)				
9-3	Talc (10)	9-10	Mordenite (9)		
9-2-9-1	Pyrophyllite (10)	9-05-8-97	Heulandite-clinoptilolite (6-10)		
8-5	Smectite, glycol (4)	8-5-8-2	Amphiboles (10)		
		7-94-7-89	Heulandite clinoptilolite (2-6)	7-6	Gypsum (10)
7-35-7-25	Serpentine (10)				
7-2-7-1	Chlorite (6-10) Al-serpentine (10)				
7-15	Kaolinite (10)				
		6-61	Mordenite (9)	6-26	Lepidocrocite (10)
				6-11	Boehmite (10)
				6-01	Bassanite (10)
				5-97-5-93	Jarosites (2-5)
		5-61	Analcime (6)	5-49	Mirabilite (10)
		5-39	Mullite (5)		
5-05-4-95	Muscovite (4-5)			5-10-5-06	Jarosites (7-10)
		4-85	Analcime (2)	4-85	Gibbsite (10)
4-8	Vermiculite (2)			4-77	Brucite (9)
4-78-4-68	Chlorites (4-8)			4-77	Mirabilite (5)
4-66-4-56	Smectite (5)	4-68-4-64	Heulandite-clinoptilolite (2-7)	4-73-4-66	Spinel (2)
4-66	Talc (3)				
4-60-4-57	Serpentines (3-6)				
4-60	Vermiculite (5)				
4-55	Talc (3)				
4-50-4-47	Palygorskite (5)	4-43	Zircon (5)	4-37	Gibbsite (5)
	Sepiolite (3)				
4-49-4-45	Mica, dioctahedral (5-9);				
	Smectite, dioctahedral (5)				
4-48-4.44	Kaolinite (4-8)				
4-44	Halloysite (9)	4-33-4-30	Opal-CT (7)	4-28-4-27	Gypsum (5)
4-36	Kaolinite (7) Dickite (7)	4-26	Quartz, low (3)	4-26	Vaterite (7)

4-31	Sepiolite (4)	4-23-4-21	K-feldspars (6)	4-18-4-15	Goethite (10)
		4-21-4-04	K-Na feldspars (6-7)		
		4-11-4-09	Opal-CT (10)		
		4-04-4-02	Na and Ca feldspars (5-8)		
		4-00	Mordenite (9)	3-99	Diaspore (10)
3-89	Muscovite $2M_1$ (4)	3-97-3-95	Heulandite-clinoptilolite	3-90	Baryte (6)
		3-83-3-70	Feldspars (7)	3-85	Sulphur (10)
3-66	Muscovite $1M$ (6)			3-73	Ilmenite (5)
3-66-3-61	Serpentine (3-6)			3-67	Hematite (3)
3-60-3-50	Chlorite (7-10) Al-serpentine (4)	3-67-3-62	Na and Ca-feldspars (2-4)	3-65	Jarosites (4)
3-60-3-58	Vermiculite (3)				
3-59-3-58	Kaolinite (7)	3-48	Mordenite (10)	3-52	Anatase (10)
		3-43	Analcime (10)	3-48	Corundum (8)
3-40	Smectite, glycol (5); Halloysite – 10 Å (5)	3-42	Sillimanite (10)	3-44	Sulphur (4), Baryte (10)
		3-39	Mullite (10) Mordenite (9)	3-40	Aragonite (10)
3-37-3-34	Sepiolite (4)	3-34	Quartz, low (10)	3-36	Graphite (10)
		3-31-3-29	K-feldspars (10)	3-32	Baryte (10)
		3-30	Zircon (10)	3-30	Vaterite (10)
		3-26-3-25	Ca-feldspars (3-5)	3-27	Aragonite (5)
		3-26-3-23	K-feldspars, 2 lines (4-10)	3-25	Rutile (10)
3-24	Palygorskite (5-10)	3-25-3-15	Pyroxenes (4-10)	3-21	Sulphur (6)
3-21	Muscovite $2M_1$ (4)	3-21-3-15	Na and Ca feldspars, 2 or 3 lines including strongest (2-10)	3-15	Sylvite (10) Fluorite (9)
		3-13-3-12	Ca-feldspars, albite (2-4)	3-13-3-11	Jarosites (7-9)
3-12	Talc (6)	3-13-3-05	Amphiboles	3-12	Pyrite (4)
3-10	Smectite, Na (5)			3-10	Baryte (10)
				3-09-3-06	Jarosites (7-10)
3-07	Muscovite $1M$ (5) Pyrophyllite (10)	3-04-2-89	Plagioclase feldspars, 2, 3, or 4 Lines (1-3)	3-08-3-06	Gypsum (6)
3-0	Muscovite, $2M_1$ (4)	3-02-2-94	Pyroxenes (4-10)	3-04	Calcite (10) Vaterite (10)
3-0	Smectite, Mg, Ca (4-7)	2-99	K-feldspars, monoclinic (5)	3-00	Bassanite (10)
		2-99-2-96	Heulandite-clinoptilolite (5-8)	2-97-2-95	Magnetite-maghemite (3)
		2-93	Analcime (5)	2-89	Dolomite (10)
2-88	Vermiculite (4)	2-91-2-87	Pyroxenes (4-10)	2-90-2-86	Spinels (4)
2-87	Muscovite $2M_1$ (4)			2-82	Halite (10)
2-86-2-82	Vermiculite (4)	2-81-2-77	Olivine (6-10)	2-81-2-77	Apatites two lines (6-10)
				2-80	Bassanite (5)
		2-75-2-69	Amphibole (10)	2-79	Siderite (10)
				2-73	Vaterite (10)
				2-72-2-69	Apatites (6-10)
				2-71	Pyrite (10)
2-66-2-64	Biotite (8) Serpentine (5)	2-69	Analcime (2) Mullite (4)	2-69	Hematite (10)
2-60-2-55	Smectite, Muscovite (4-10) Chlorite (1-6)	2-60-2-53	Pyroxene (5-10)	2-55	Corundum (9)
2-56	Kaolinite (6)			2-53-2-51	Magnetite-maghemite (10)

2-46-2-43	Chlorite (2-8)	2-49-2-46	Olivine (7-10)	2-51	Hematite (7)
2-39	Kaolinite (8)			2-49	Rutile (5)
2-375	Serpentines (8)			2-47-2-44	Spinel (10)
				2-45-2-43	Goethite (6)
				2-42	Pyrite (7)
				2-37	Brucite (10)
		2-30-2-25	Olivine (2-4)	2-35	Boehmite (6)
		2-20	Mullite (6) Sillimanite (6)	2-21	Pyrite (5) Anhydrite (2)
2-16-2-13	Serpentines (2-8)			2-12	Baryte (8)
		2-07	Zircon (2)	2-07	Pyrrhotite (10)
2-05-1-99	Chlorites (2-6)			2-06	Vaterite (10)
2-01-1-99	Muscovite (3-5)			2-03	Graphite (5)
1-989	Kaolinite (6)			1-994	Halite (5)
				1-977	Aragonite (6)
				1-931	Fluorite (10)
1-870	Talc (4)	1-817	Quartz, low (2)	1-838	Hematite (3)
		1-77-1-75	Olivine (4)	1-726	Ilmenite (6)
1-72-1-68	Smectite (1-5)	1-712	Zircon (4)	1-692	Hematite (5)
				1-687	Rutile (6)
1-662	Kaolinite (7)			1-647	Fluorite (4)
				1-633	Pyrite (10)
1-619	Kaolinite (6)			1-617-	Magnetite-maghemite
1-58-1-52	Chlorite (2-7)			1-614	(3)
				1-601	Corundum (8)
				1-576-	Spinels (4)
				1-555	
				1-573	Brucite (4)
1-54-1-49	Smectite (2-6)	1-541	Quartz (2)		
1-537	Vermiculite (5)				
1-527	Talc (5)	1-525	Mullite (5)	1-485-	Magnetite-maghemite
		1-519	Sillimanite (3)	1-474	(4)
1-503-				1-484	Hematite (2)
1-499	Muscovite (4)			1-469	Ilmenite (3)
1-489	Kaolinite (8)			1-452	Hematite (3)
1-484	Halloysite (5)			1-448-	Spinels (6)
1-452	Kaolinite (4)			1-429	

1179

1180

1181
1182

Annex II. Main IR vibration bands of common clay minerals (after [113])

Clay mineral	Formula	Wavenumber, cm ⁻¹ *
Kaolinite	Al ₂ Si ₂ O ₅ (OH) ₄	3693s, 3655sh, 3620, 1115s, 1090s, 1032s, 1006s, 939, 914s, 792, 753, 696, 642, 600sh, 536s, 470s, 429
Dickite	Al ₂ Si ₂ O ₅ (OH) ₄	3708, 3655, 3625, 1118s, 1080, 1033s, 1004s, 965sh, 937, 914, 795, 755w, 697, 600sh, 534s, 467s, 425
Nacrite	Al ₂ Si ₂ O ₅ (OH) ₄	3710, 3660, 3640, 1120s, 1100s, 1036s, 1003s, 930sh, 913, 799w, 754w, 696, 600sh, 535s, 468s, 424
Halloysite-10Å	Al ₂ Si ₂ O ₅ (OH) ₄ ·2H ₂ O	3615, 3525w, 3395, 1630w, 1075s, 1037s, 1023s, 827w, 788, 743w, 676, 617w, 590sh, 490sh, 468s
Halloysite	Al ₂ Si ₂ O ₅ (OH) ₄ ·nH ₂ O	697w, 3620, 3380, 1630w, 1090sh, 1028s, 1020sh, 913, 790sh, 750w, 671, 533, 495sh, 471s, 435sh
Pyrophyllite	Al ₂ Si ₄ O ₁₀ (OH) ₂	3678, 1120s, 1068s, 1050s, 950s, 854, 836, 814, 737w, 620, 578, 539s, 519, 481s, 458, 414
Saponite	(Ca _{0.5} ,Na) _{0.3} (Mg,Fe ²⁺) ₃ [(Si,Al) ₄ O ₁₀](OH) ₂ ·4H ₂ O	3635, 3430sh, (3330), 1650w 1002s, 770w, 730w, 665, 459s
Hectorite	Na _{0.3} (Mg,Li) ₃ (Si ₄ O ₁₀)(F,OH) ₂	3682w, 3640w, 3450w, 1625w, 1065sh, 1010s, 900sh, 701, 687, 677, 656, 520sh, 464s
Stevensite	Ca _x Mg ₃ [(Si,Al) ₄ O ₁₀](OH) ₂ ·nH ₂ O (x 0.15, n 2)	3450, 1638, 1023s, 669, 525sh, 470s, 453s
Montmorillonite	(Na,Ca) _{0.3} (Al,Mg) ₂ (Si ₄ O ₁₀)(OH) ₂ ·nH ₂ O	3620, 3430w, 1620w, 989, 923s, 912s, 800w, 701s, 607, 540s, 486s
Beidellite	(Na,Ca _{0.5} ,K) _x Al ₂ [(Si,Al) ₄ O ₁₀](OH) ₂ ·nH ₂ O (x 0.3)	3590, 3415, 1640w, 1110sh, 1033s, 1010sh, 935sh, 912, 697w, 534s, 473s, 423s
Nontronite	(Na,Ca) _x (Fe ³⁺ ,Al,Mg) ₂ [(Si,Al) ₄ O ₁₀](OH) ₂ ·nH ₂ O (x 0.3, n 4)	557, 3390, 3240sh, 1650sh, 1632, 1100sh, 1021s, 940sh, 847, 817, 745w, 675, 585, 492s, 450sh, 430s, 380s
Vermiculite	(Mg,Fe,Al) ₃ (Si,Al) ₄ O ₁₀ (OH) ₂ ·4H ₂ O	3550sh, 3375, 3250sh, 1657, 1070sh, 991s, 819w, 730sh, 710sh, 680sh, 657, 510sh, 450s, 420sh
Illite	K _{0.65} Al ₂ (Si _{3.35} Al _{0.65} O ₁₀)(OH) ₂	3620, 3420, 1665w, 1635w, 1080sh, 1023s, 1000sh, 915, 825sh, 754w, 700w, 605sh, 525s, 471s, 425sh
Glauconite	K _{1-x} (Fe ³⁺ ,Mg,Fe ²⁺ ,Al) ₂ [Si ₃ (Si,Al)O ₁₀](OH) ₂	3645sh, 3600sh, 3560, 3540sh, 3365, 3240sh, 1630w, 1120sh, 1029s, 995sh, 877, 819w, 677w, 489s, 460s, 431sh
Phlogopite	KMg ₃ (Si ₄ AlO ₁₀)(OH) ₂	3695, 3675, 3375, 1740w, 1660sh, 1640, 995s, 818, 760sh, 726, 689, 650, 606, 520sh, 490sh, 459s, 430sh
Muscovite	KAl ₂ (Si ₃ AlO ₁₀)(OH) ₂	3570, 3385, 1610w, 1070sh, 1023s, 999s, 906, 826, 744w, 660w, 600sh, 520s, 469s, 417.
Clinochlore	(Mg,Al) ₆ (Si,Al) ₄ O ₁₀ (OH) ₈	3670, 3615sh, 3580, 3440, 1085sh, 1061, 996s, 961s, 815, 648, 526, 490sh, 455s, 437s, 415sh
Clinochlore	(Mg,Al) ₆ (Si,Al) ₄ O ₁₀ (OH) ₈	3630sh, 3570, 3440sh, 1635w, 1045sh, 993s, 962s, 812w, 795w, 710sh, 650, 610sh, 446s
Chamosite	(Fe,Al,Mg) ₆ (Si,Al) ₄ O ₁₀ (OH) ₈	3540, 3360, 3220sh, 981s, 746, 659, 610, 446s, 420sh
Sepiolite	Mg ₄ (Si ₆ O ₁₅)(OH) ₂ ·6H ₂ O	3625sh, 3577, 3395, 3230sh, 1654, 1625sh, 1205, 1065sh, 1019s, 980sh, 782w, 728w, 686, 643, 530sh, 495sh, 466s, 440sh, 420sh
Palygorskite	(Mg,Al) _{2+x} (Si ₄ O ₁₀)(OH) ₂ ·4H ₂ O	3615, 3580, 3415, 3280sh, 1660, 1197, 1119, 1083, 1040s, 986s, 909w, 870w, 680sh, 643w, 570, 540sh, 511, 484s, 438

*s = strong; w = weak; sh = shoulder

1183